EUROPEAN ORGANIZATION FOR NUCLEAR RESEARCH

CERN/EF 82-3
25 February 1982

EXPERIMENTS AND DETECTORS AT THE CERN $\bar{p}p$ COLLIDER

A. Minten

CERN, Geneva, Switzerland

PREFACE

This lecture is one of a series of three around the CERN $\bar{p}p$ Collider. The three are, in logical order:

(i) Some Accelerator Aspects of $\bar{p}p$ Colliding Beams, by R. Johnson [1];
(ii) Physics at Collider Energy, by R. Horgan and M. Jacob [2];
(iii) Experiments and Detectors at the CERN $\bar{p}p$ Collider (this lecture).

This present lecture is intended for students preparing a thesis in the field of particle physics. It is composed of three main sections along the following subjects:

- definition of the goals of $\bar{p}p$ experiments, and specifications of detector requirements,
- a short survey of detection methods applied,
- detectors of the five $\bar{p}p$ experiments.

Lectures presented at the International School of
Elementary Particle Physics, Kupari-Dubrovnik (Yougoslavia)
September 1981

0901F/AM/ef

TABLE OF CONTENTS

1. INTRODUCTION

The $\bar{p}p$ collider [1]

In the year 1981 a new physics facility starts operation at CERN: the SPS $\bar{p}p$ Collider, proposed in 1977 by C. Rubbia. It implies the simultaneous storage of p and $\bar{p}$ in the SPS ring. Both beams circulate at a continuous magnetic field corresponding to a beam energy of 270 GeV, and they collide head-on with a c.m. energy

$$\sqrt{s} = E_1 + E_2 = 540 \text{ GeV} .$$

This energy could be produced by an antiproton beam with energy E_1 impinging on a proton target at rest. From

$$\sqrt{s} = \sqrt{(E_1 + m_p)^2 - p_1^2} \simeq \sqrt{2E_1 m_p}$$

follows E_1 = 155 000 GeV, which outside the range of presently known accelerator technologies.

Methods and techniques used, namely:

- production of antiprotons by the CERN Proton Synchrotron (PS),
- "cooling" of antiprotons in the Antiproton Accumulator (AA),
- storing of (anti)protons in the Super Proton Synchrotron (SPS),

are treated in the lectures by R. Johnson [1].

2. $\bar{p}p$ EXPERIMENTS

2.1 Luminosity and Rates

The luminosity L of two intercepting bunches (1) and (2) of particles is defined by

$$L \text{ [cm}^{-2}\text{s}^{-1}\text{]} = \text{density (1) [cm}^{-3}\text{]} \cdot \ell_1 \text{ [cm]} \cdot \text{flux (2) [s}^{-1}\text{]}$$

- for a cylindrical target bunch (1) with length ℓ_1 and cross section area A,
- for a penetrating projectile bunch (2) circulating in the storage ring with circumference $2\pi R$, and

- for n_1 bunches in direction of (1) and n_2 bunches in (2), with n_b, the smaller of both, we obtain

$$L = \frac{N_1}{A\ell_1} \ell_1 \frac{N_2 c}{2\pi R} n_b ,$$

$$= \frac{N_1 N_2}{A} \frac{c}{2\pi R} n_b .$$

We see that the luminosity is independent of the bunch length ℓ, but is geometrically determined by the effective overlap area A, with

$$\frac{1}{A} = \frac{\int \rho_1(x,y)\ \rho_2(x,y)\ dx\ dy}{\int \rho_1(x,y)\ dx\ dy \int \rho_2(x,y)\ dx\ dy}$$

and with $\rho(x,y)$ the particle density distribution in the beam. A, can be experimentally obtained by a <u>two</u>-dimensional (x,y) relative beam scan. This method, proposed in 1968 by S. Van der Meer, is commonly used on <u>one</u> dimension at the CERN ISR.

Inserting the design values into the expression for L, namely

$N_1 = 10^{11}$ antiprotons/bunch,
$N_2 = 10^{11}$ protons/bunch,
$A = 0.003$ cm^2 effective area,
$R = 10^5$ cm SPS radius,
$n_b = 6$ bunches of $p(\bar{p})$,

we obtain the design luminosity

$$L_{design} = 10^{30}\ cm^{-2}\ s^{-1}.$$

Presently reached (10 December 1981), was a luminosity of 10^{27} cm^{-2} s^{-1}. The measured <u>luminosity life time</u> was $\sim$ 16 h. The <u>event rate</u> R for a reaction with cross section σ [cm^2] is

$$R\ [s^{-1}] = \sigma \cdot L .$$

The <u>number of events</u> (NEV) within an experiment over a (reasonable) running time is

$$NEV = \sigma \int L\ dt .$$

A reasonably effective running time seems to be 100 days ≈ 10^7s. For $L = 10^{29}$ cm^{-2} s^{-1}, this corresponds to 1 event per picobarn (1 barn = 10^{-24} cm^2, 1 pbarn = 10^{-36} cm^2).

2.2 Reactions and cross sections [2,3]

We consider two colliding beams of antiprotons and protons, both with momentum p = 270 GeV/c. In the quark picture this corresponds to two beams of (anti) triquark systems ($\bar{u}\bar{u}\bar{d}$) and (uud), each quark with a fraction of 270 GeV/c. The triquarks collide, react and form final states. In order to design our detectors and to define their parameters, we select four representative final state configurations.

(a) $\bar{p}p \to$ anything

The sum of all final states gives the total cross section, which is expected to be around 60 mb (60 . 10^{-27} cm^2). In addition, a sample of "normal" event types yields information on the particle multiplicity <n>, on the multiplicity distribution f(n), and on angle and rapidity distributions $d\sigma/d\Omega$ and $d\sigma/dy$.

(b) Elastic scattering $\bar{p}p \to p\bar{p}$

Coherent scattering of all three quarks on the three antiquarks gives the elastic cross section. The total elastic cross section is expected around 10 mbarn (10^{-26} cm^2).

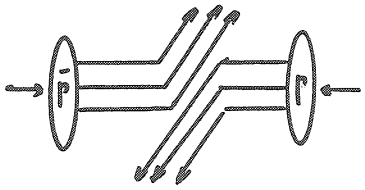

(c) Quark scattering

$\bar{p}p \to \bar{q}q$ + "spectators"
↳ jets

Pointlike scattering of one antiquark on one quark, the two scattered quarks forming two jets of secondary hadrons, and the spectator quarks reacting similar to a "normal" event (a).

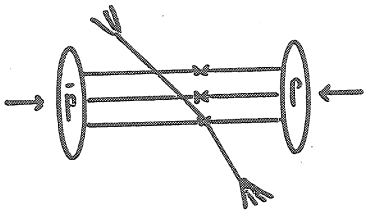

The quark scattering cross section, depending on the quark's transverse momenta, is of the order of μbarns (10^{-30} cm^2).

(d) Quark annihilation $\bar{p}p \to V$ + spectators

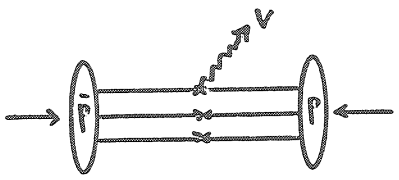

One antiquark and one quark annihilate and form an intermediate vector boson γ, Z^0 or $W^{\pm}$.

$$\bar{u}u,\ \bar{d}d \to \gamma,\ Z^0 \qquad \bar{u}d \to W^-,\quad \bar{d}u \to W^+$$

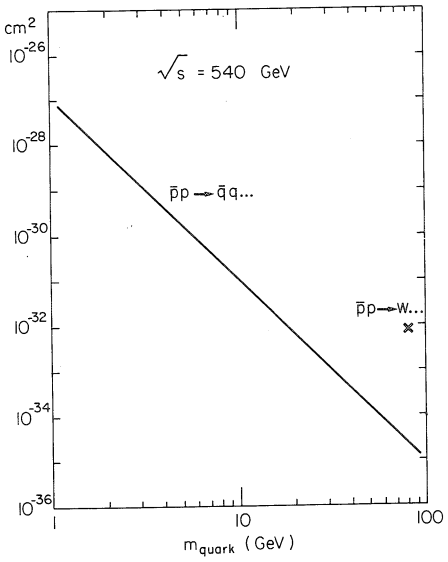

Fig. 1

The intermediate vector bosons decay in turn into pairs of quarks ($\bar{q}q$) or pairs of leptons (ν, e, μ).

The cross section depends on the mass of the intermediate state and is expected to be some 10^{-33} cm² for the Z^0, $W^{\pm}$ (fig. 1).

2.3 Production and decay of Z^0, $W^{\pm}$ [2,3]

We consider production and decay of Z^0. Production occurs via quark annihilation

$$\bar{u}u,\ \bar{d}d \to Z^0$$

with a Z^0 mass of 89 GeV, the expected production cross section being

$$\sigma(\bar{p}p \to Z^0 + \ldots) = 1.6\ 10^{-33}\ \text{cm}^2.$$

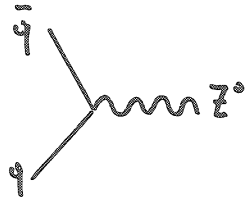

Z^0 decays into lepton or quark pairs, the latter giving origin to two hadron jets

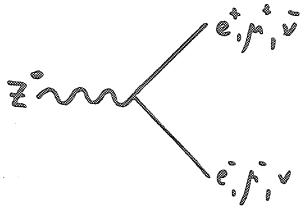

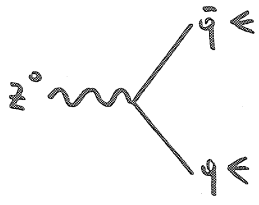

The expected total decay width is $\Gamma = 2.5$ GeV, which corresponds to a lifetime $\tau = 2.6\ 10^{-25}$ s, from $\tau \cdot \Gamma = h$.

The expected branching ratios (BR) into different decay channels are

$Z^0 \to e^+e^-$ BR = 0.03

$\to \mu^+\mu^-$ = 0.03

$\to \bar{\nu}\nu$ = 0.06

$\to \bar{q}q \to$ hadrons BR = 0.8

The rate for a specific channel is now $R = \sigma L BR$. The experiment consists of detection of e^+e^-, $\mu^+\mu^-$ pairs and of the study of their effective mass spectrum

$$M^2_{eff} = 2 E_1 E_2 (1-\cos\theta_{12}) .$$

We now turn to the production of the charged $W^\pm$ bosons

$\bar{u}d \to W^-$ and $\bar{d}u \to W^+$

with an expected mass of 79 GeV, and a cross section

$$\sigma(\bar{p}p \to W^- + \ldots) = \sigma(\bar{p}p \to W^+ + \ldots) = 3.6\ 10^{-33}\ cm^2 ,$$

$W^\pm$ decays into lepton and quark pairs, with only one charged lepton.

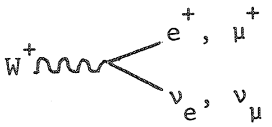

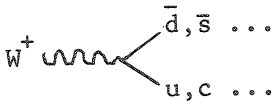

Decay width and branching ratios are expected to be similar to those of Z^0.

The experiment consists of detecting the p_T spectrum of one single lepton. One expects an apparent unbalance of p_T, due to the undetected neutrino. One makes use of the "Jacobian peak", which results from fig. 2:

- W produced with limited (small) p_T,
- W decaying with the charged lepton mostly around 90° with respect to the $\bar{p}p$ axis,
- the decay leptons having around 40 GeV/c momentum.

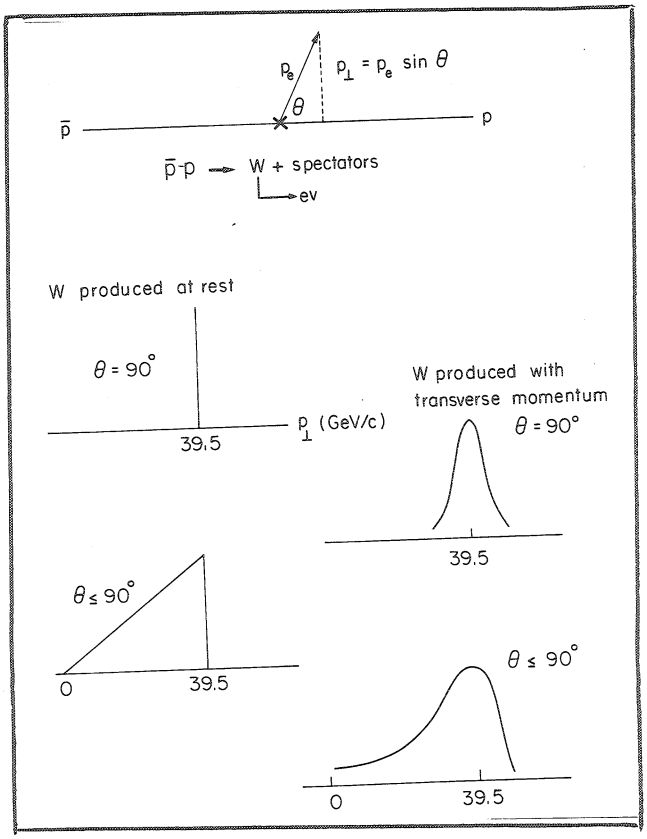

Fig. 2

2.4 Backgrounds

We have to ask the question whether there are other sources of single (or pairs of) high p_T leptons which might simulate decays of $W^{\pm}$ (or Z^0).

An obvious source is the (semi)-leptonic decay of unstable hadrons π, K, Λ, C, B etc. Since the masses of these lepton parents are comparatively small, the hight p_T must stem from the production process of the parent. For a quantitative study of this background, the measured invariant cross section for high p_T hadrons

$$E \frac{d^3\sigma}{dp_3} = f(y)\, p_T^{-n} \quad (y \text{ rapidity, } n = 4 \text{ at ISR energies})$$

has to be extrapolated to collider energies and transverse momenta of $\sim$ 40 GeV/c. Taking as input these extrapolated cross sections for hadron parents, and estimated cross sections for $W^{\pm}$, Z^0, and applying the known decay kinematics, we obtain lepton spectra as shown in fig. 3.

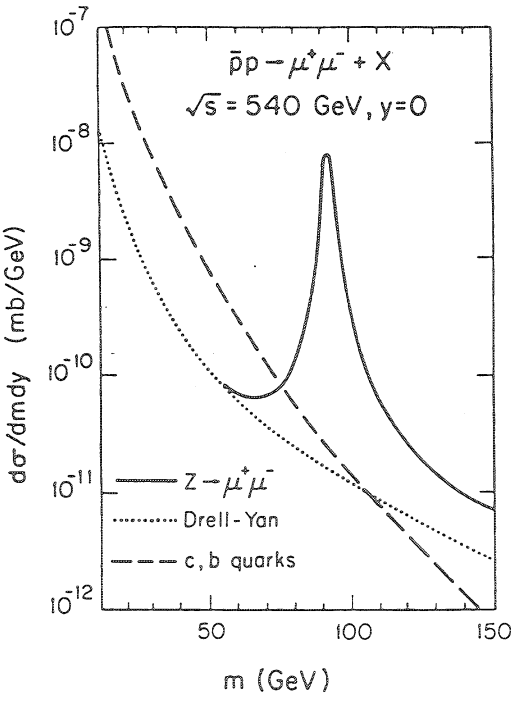

The lepton-pair spectrum in $\bar{p}p$ collisions at $\sqrt{s}$ = 540 GeV, y = 0, with different background contributions

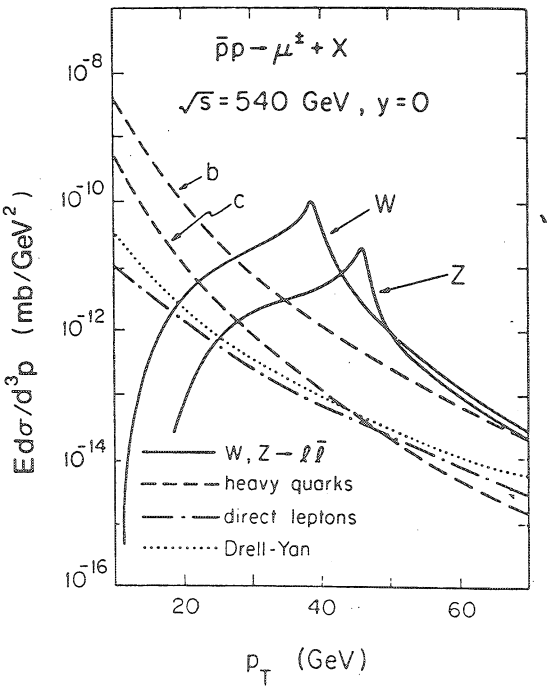

Single-lepton invariant cross-section in $\bar{p}p$ collisions at $\sqrt{s}$ = 540 GeV, y = 0, with various background contributions from Drell-Yan processes, almost-real high-p_T photons, and c and b quarks

Fig. 3 (ref. [3])

We conclude that $W^{\pm}$, $Z^0 \to$ leptons can be detected.

2.5 The "typical" event

We define a set of "typical" events for the reactions listed under 2.3 in order to optimize the parameter of an "ideal" detector. The "typical" event is characterized by:

- a charge multiplicity $\langle n \rangle_{ch} \simeq 40$;
- longitudinal momenta up to 270 GeV/c (elastic scattering);
- limited transverse momenta of $\langle p_T \rangle = 0.3$ GeV/c, but exceptional transverse momenta of 40 GeV/c from decays of heavy particles (Z^0, $W^{\pm}$);
- jets of charged and neutral secondary hadrons;
- presence of photons, electrons and muons.

The events can be represented in a "Peyrou plot" (fig. 4), i.e. a p_L - p_T display of three-momenta. Note that the ratio of $p_L^{max}:\langle p_T \rangle \simeq 10^3$. Note further that the population in p_L and p_T decreases roughly exponentially with increasing secondary p_L and p_T.

2.6 The "ideal" detector

Which are the measurable quantities, and with which instrument are they measured?

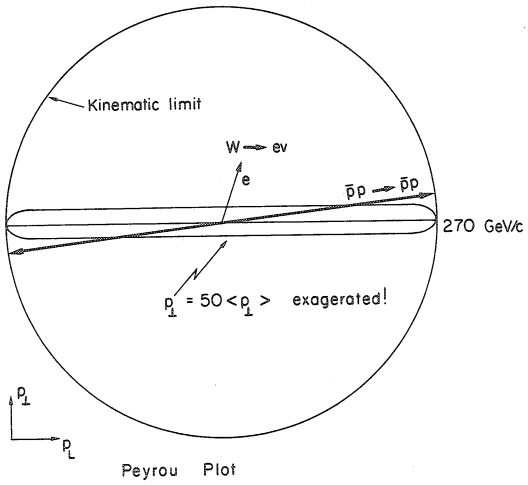

Fig. 4

(a) charge and momentum are determined from curvature in a magnetic field;

(b) trajectory (angles, momentum, i.e. $\bar{p}$) are determined by position detectors, usually multiwire proportional or drift track chambers;

(c) energy and direction of photons (and identity of electrons (sect. 3.7) are determined by means of photon calorimeters;

(d) energy and direction of neutral hadrons, K^0 and neutrons and total energy of hadron jets are determined by means of hadron calorimeters;

(e) identity of hadrons (π, K, p) in certain momentum regions can be determined by means of ionization measurements;

(f) identity of muons can be determined from their penetration of matter.

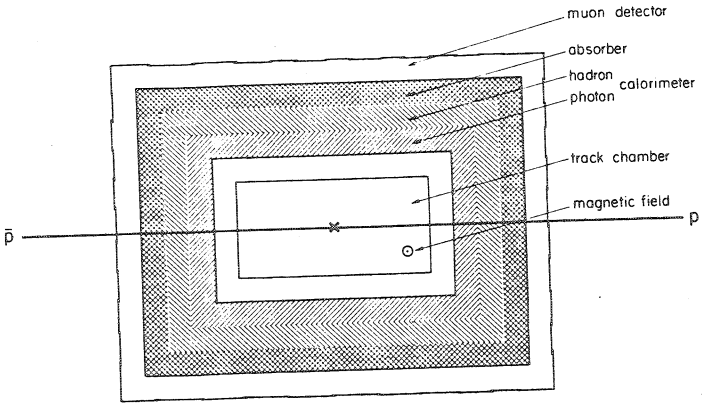

Fig. 5

The "ideal" detector which combines most of the above specifications, is shown in fig. 5.

2.7 Detector parameters

A detector system, and in consequence an experiment, is characterized by the following parameters:

(a) Resolution is defined as $\Delta\theta/\theta$ or $\Delta p/p$ for a measured quantity θ or p, or as $\Delta M/M$ for a calculated quantity M. Here $\Delta\theta$ (Δp, ΔM) is the standard deviation σ in a Gaussian distribution of the measurements of θ (p,M).

(b) Acceptance (ACC) is defined in its most elementary form as geometrical acceptance $\Delta\Omega//4\pi$, or in phase space

$$ACC = \int_{detector} d\,p^3 \Big/ \int_{physics} d\,p^3 .$$

Another definition is the acceptance for a specific reaction or final state, where the integral includes the weight from the differential cross section for the reaction (n) with σ_n as the partial cross section

$$ACC = \int_{detector} \frac{d^3\sigma_n}{dp^3} \Big/ dp^3/\sigma_n \; ;$$

(c) sensitivity, defined as the number of events per unit cross section detected. From $NEV = \sigma_n \cdot BR\ ACC \int L\,dt$ sensitivity [events/cm^2] = $BR\ ACC \int L\,dt$;

(d) selectivity and rejection, the possibility to select from a data set the wanted events and to reject the unwanted ones. For example, to select one $Z^0 \to e^+e^-$ with BR = 0.03 and $\sigma_n = 1.6 \cdot 10^{-33}$ cm^2 against all other events with a total cross section of 60 mb, one needs a

$$\text{selectivity} = \frac{BR \cdot \sigma_n}{\sigma_{tot}} = 8.10^{-10} .$$

3. DETECTION METHODS

3.1 Magnetic field configuration

The purpose of the magnetic field is to determine the curvature of a particle trajectory and thereby charge and momentum of the particle. The curvature radius is

$$R\ [m] = \frac{p\ [GeV/c]}{0.3\ B\ [Tesla]}\ .$$

The quantity measured in the track detector is the sagitta

$$s = \frac{L^2}{8R}$$

The resolution of the measurement is [5]

$$\frac{\Delta s}{s} = \frac{\Delta p}{p} = \frac{8}{0.3}\ \frac{p}{L^2 B}\ \sigma \sqrt{\frac{11}{N+5}}\ ,$$

where σ is the r.m.s. error of position measurement in the track chamber, and the square root contains a statistics factor with N as the number of position measurements (fig. 6).

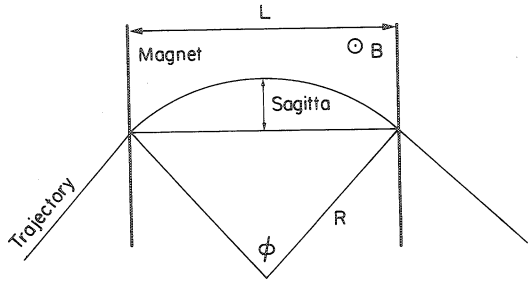

Fig. 6

We consider three magnetic field configurations for collider experiments:

(a) Solenoid, with a longitudinal homogeneous field, parallel to the beam direction, therefore no distortion to the beams to first order, but bending $\vec{p} \times \vec{B} \propto \sin\theta$ and therefore ineffective for forward particles, most abundant in hadronic interactions. The solenoid configuration was not retained for the $\bar{p}p$ detectors.

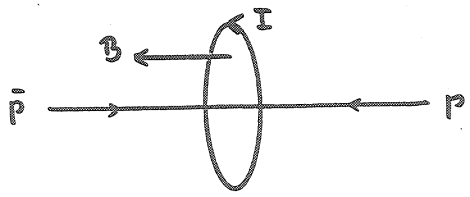

(b) Dipole, with a transverse homogeneous field B_z, therefore deflecting also the circulating beams and requiring compensator magnets. The bending power is proportional to $\vec{p} \times \vec{B}_z$ and therefore dependent on the angles θ and ϕ, but it is fully effective in the forward directions. The dipole configuration was retained for the UA1 detector.

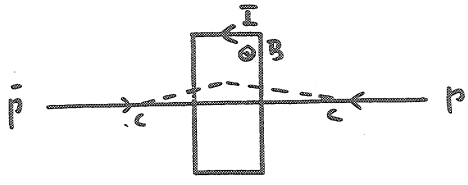

(c) Toroid, with a circular field decreasing as 1/r, but full cancellation on the beam axis and therefore, to first order, no distortion on the beams. Bending power is independent of production angles, but the drawback is the presence of an electric conductor around the beam line. Toroidal magnets were retained for a limited acceptance region in the forward spectrometers of the UA2 detector.

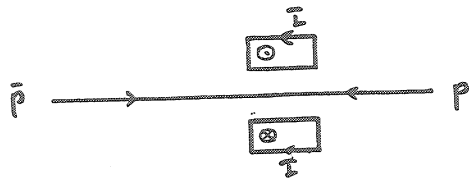

3.2 Multiwire Proportional Chambers (MWPC)

The purpose of wire chambers is the detection of charged and therefore ionizing particles. The principle of operation is as follows (fig. 7):

- a charged particle traverses a gas layer (e.g. 1 cm of 60% argon and 40% isobutane) and creates ion-electron pairs by ionization;
- positive ions and negative electrons drift in an electric field to the respective electrode;
- the very high electric field near the thin anode wire (∿ 20 μm ∅) initiates through gas amplification the formation of an avalanche;
- electrons from the avalanche are collected on the anode, and ions migrate to the cathode;
- the migration of positive ions away from the anode wire frees a negative charge signal on the anode and positive induced signals on the cathode, and on the adjacent anode wires.

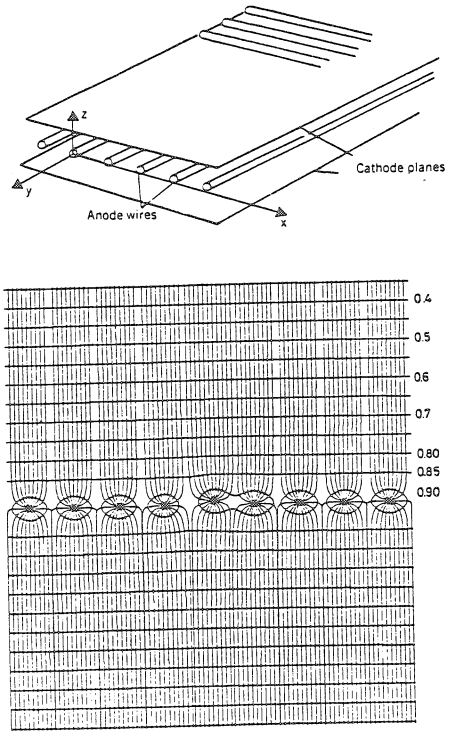

Fig. 7 (ref. [4])

The successive stages of the process are reflected in the following numbers:

- primary charge from ionization: 10^2 electrons in 1 cm argon,
- gas amplification: 10^4,
- charge deposit on the anode wire: 10^6 electrons $\simeq 10^{-13}$ Coulomb,
- electrical current during 10^{-7} s: $10^{-13}/10^{-7} \simeq 10^{-6}$ A,
- electrical voltage over 1 KΩ: 10^{-3} V,

A second coordinate may be obtained in the same detection gap by two methods:

(a) Detection of the induced positive pulse on a subdivided cathode plane (wires or strips), where the subdivision is inclined or orthogonal to the direction of the anode wires. The position of the avalanche is determined in the centre of gravity of the induced pulses.

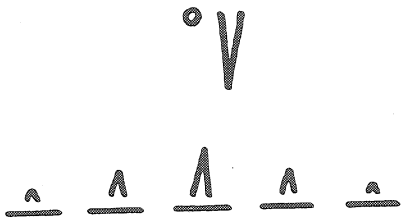

(b) Resistive charge division of the deposited electron charge and detection of two signals at either end of the anode wire. This has the additional advantage of giving one space point instead of two coordinates, thus avoiding ambiguities in case of multitrack traversal.

3.3 Drift Chambers (DC)

The drift chamber is a MWPC, in which the configuration of the electric field is chosen in such a way that electrons drift with constant drift velocity V_D to the anode wire. For a known velocity, the position can then be determined by measurement of the drift time with respect to an external time zero, given by a scintillator (fig. 8). For argon-isobutane mixtures we have $V_D \simeq 50$ mm/μs, and $X = V_D t_D$.

The resolution is limited by the dispersion of drift paths of electrons and by diffusion of electrons in the gas.

One intrinsic problem of the drift chamber is its right-left-ambiguity, i.e. the impossibility to determine in a simple geometry the side from which

the electrons arrive on the anode. This drawback can be avoided in special field configuration.

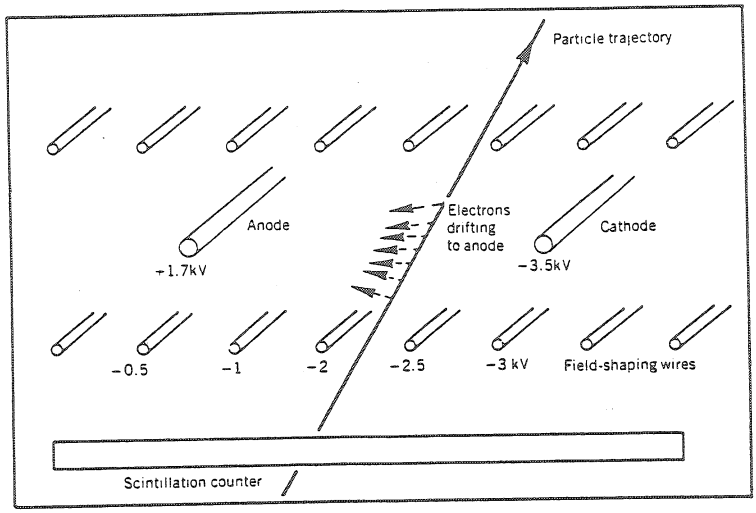

Fig. 8 (ref. [4])

3.4 Pictorial drift chambers [6]

The main properties of so-called pictorial or image chambers are the following:

- Measurement of many points of a particle track in order to obtain redundancy for track finding in high multiplicity events.
- Measurement of space points of the trajectory in order to avoid ambiguous solutions in case of several tracks traversing the same chamber gap; a space point is usually obtained by charge division on the hit sense wire.
- Avoiding right-left ambiguity by proper shaping of the electric field around a sense wire so that electrons can normally drift only from one side.
- Arrangement of relative direction of magnetic and electric field in such a way that curvature and drift direction are in one plane, so that the high precision in drift time measurement ($\sim$ 200 μm) is used for momentum determination. One problem is the deflection of drifting electrons due to the magnetic field. An empirical correction must be applied.

Fig. 9 shows four generations of central detectors (CD) for collider spectrometers over the last decade.

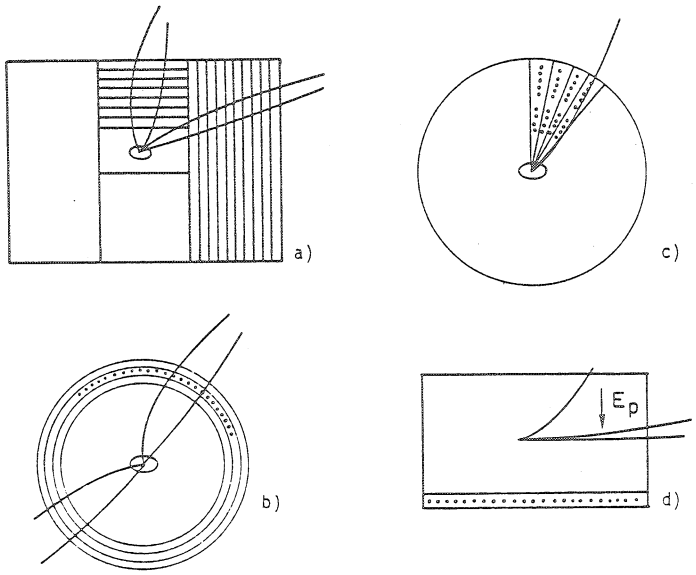

Fig. 9 (ref. [4])

3.5 Energy loss by ionization

A charged particle traversing matter looses energy by ionization of atoms. This energy loss can be used either to determine the number of ionizing (relativistic) particles (used in shower detectors), or to measure the velocity $\beta = v/c$ of the particle.

The mean energy loss in a thing (gaseous) layer of matter is

$$\frac{dE}{dx}\left[\text{MeV g}^{-1}\text{ cm}^2\right] = 0.1535\,\frac{Z}{A}\,\frac{1}{\beta^2}\left(\ln\left(\frac{2m_e c^2 \beta^2 T_{max}}{(1-\beta^2)\,I^2}\right) - 2\beta^2 + \text{corr.}\right)$$

with T_{max} the maximum energy of a δ ray contained in detector, I the mean ionization potential I [ev] $\simeq$ 10.Z, and the correction term accounting for atomic, radiation and polarization effects.

We identify two separate regions:

(i) the low energy ($\beta\gamma < 1$) non-relativistic region with

$$-dE/dx \propto \beta^{-2},$$

(ii) the high energy ($\beta\gamma >> 1$) relativistic region with

$$-dE/dx \propto \log (1-\beta^2)^{-1} = \log \gamma^2.$$

For known momentum, the particle rest mass can be identified by means of determination of β through the relation $p = m_o \beta\gamma c$ (fig. 10).

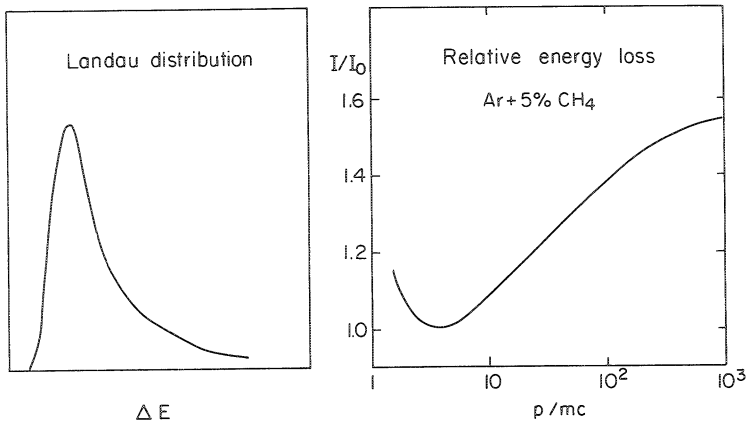

Fig. 10

3.6 Calorimeters

Calorimeters are destructive detectors which measure the "total energy" (and, if possible, position and direction) of charged and neutral particles by absorbtion. Not included in "total energy" are the rest masses of stable (p, n, e) or longliving (μ) particles. The particle (mainly kinetic) energy is converted into ionization or atomic excitation with light emission or into Cerenkov radiation. It is eventually converted into heat, which as such remains undetectable in the detection volume necessary [1 GeV = $1.6\ 10^{-10}$ Joule].

In practice, we differentiate between electromagnetic calorimeters for electrons and photons and hadron calorimeters, based on electron-photon and hadronic cascades, respectively.

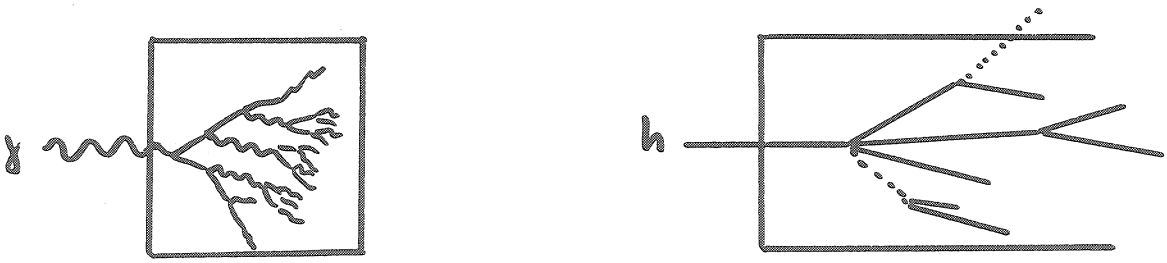

Calorimeters are described by a number of parameters:

(a) absorption length [gcm^{-2}], i.e. the measure of the mean free path of an individual cascade particle in a given material (A, Z);

(b) containment of the cascade in the calorimeter of given mass and dimensions, and its complement, leakage of cascade particles out of a finite calorimeter volume;

(c) energy resolution $\sigma(E)/E$, usually determined by statistical fluctuations of the detection mechanism and therefore $\sigma(E)/E \propto \sqrt{E}$;

(d) spacial resolution σ_x.

3.7 Electromagnetic calorimeters

The physical processes involved are bremsstrahlung and pair production

where

$$\sigma_{Bs} \simeq \sigma_{pair} = \alpha\, r_0^2\, Z^2\, \ell n\,(183\, Z^{-1/3})\ [cm^2]$$

with $\alpha = 1/137$ and $r_0 = 2.818\ 10^{-13}$ cm, the classical electron radius.

In this case the parameters are the following:

- The mean free path is the radiation length X_0

$$X_0 = 716\ A/Z^2\ \ell n(183\ Z^{-1/3})\ [gcm^{-2}]\ .$$

- The shower mechanism continues above and down to a critical energy Σ, where the energy losses of an electron from radiation and ionization become equal and below which the shower degrades

$$\epsilon = 0.55/Z\ [GeV]\ .$$

- The number of electrons (or positrons of photons) increases exponentially with a lower depth t and reaches a shower maximum at

$$t_{max} = \ell n(E_{in}/\epsilon) - 1\ [X_0];$$

beyond t_{max} the shower degrades.

- The shower is therefore contained in a depth D of

$$D = t_{max} + \text{attenuation of electrons } [X_0].$$

Fig. 11 shows the development of an electro-magnetic shower in the BEBC bubble chamber filled with a NeH mixture.

Practical electromagnetic calorimeters may be either homogeneous, with one medium for passive shower development and active shower detection, or heterogeneous sampling calorimeters with separation of the two functions:

(a) The most common homogeneous type is the lead-glass counter, where shower electrons emit Cerenkov light which is detected in a Photo-electron Multiplier (PM). The empirical value for the resolution is $\sigma(E)/E \simeq 0.1/\sqrt{E\,[GeV]}$

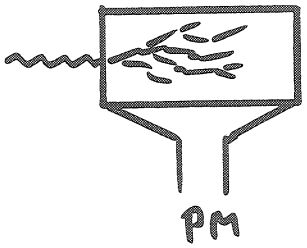

lead glass PbO + SiO_2
X_0 = 10 gcm^{-2}
ϵ = 16 MeV

(b) Sampling e.m. calorimeters are usually made of lead, interleaved with active detector. Resolution is reduced by sampling fluctuation for $n_s = E/\Delta E$ samplings, so we get $\sigma(E)/E \propto 1/\sqrt{n_s} = \sqrt{\Delta E/E}$, empirically $\sigma(E)/E \simeq 0.2/\sqrt{E\,[GeV]}$

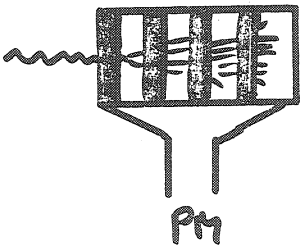

	Fe	Pb
Z	26	82
ϵ [MeV]	20	7
X_0 [gcm^{-2}]	14	6.4

The active detector in a heterogeneous calorimeter can be built in different ways: usually solid plastic scintillators undergo atomic excitation with subsequent emission of light, which is detected by means of a photomultiplier. Other techniques include ionization of a liquid (liquid argon, LA) or a gaseous medium and the detection of the corresponding electrical signal (fig. 12).

A novel method has been devised to transmit the light produced in a plastic scintillator (or radiator) to the phototube. Traditionally, this

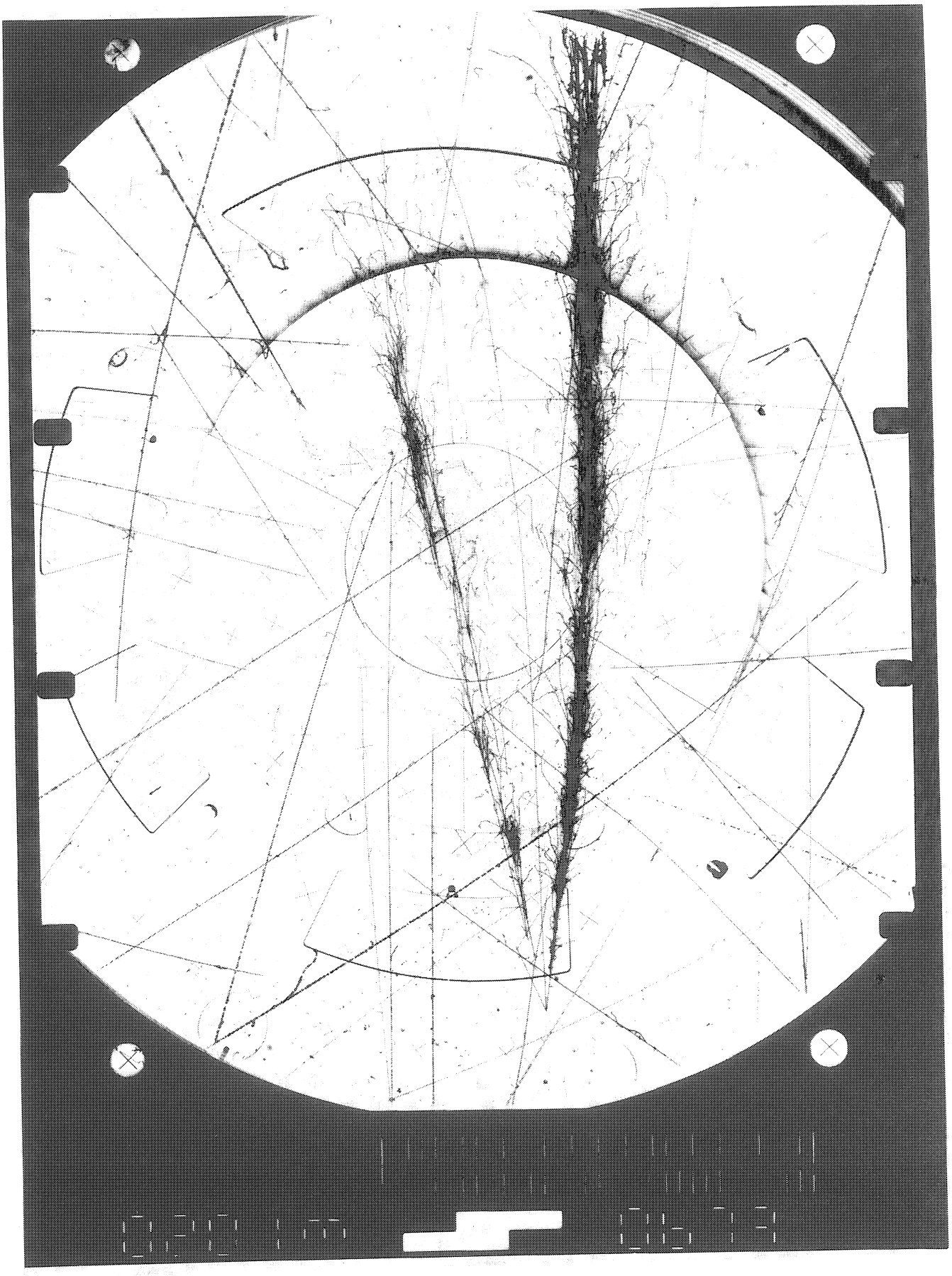

Fig. 11

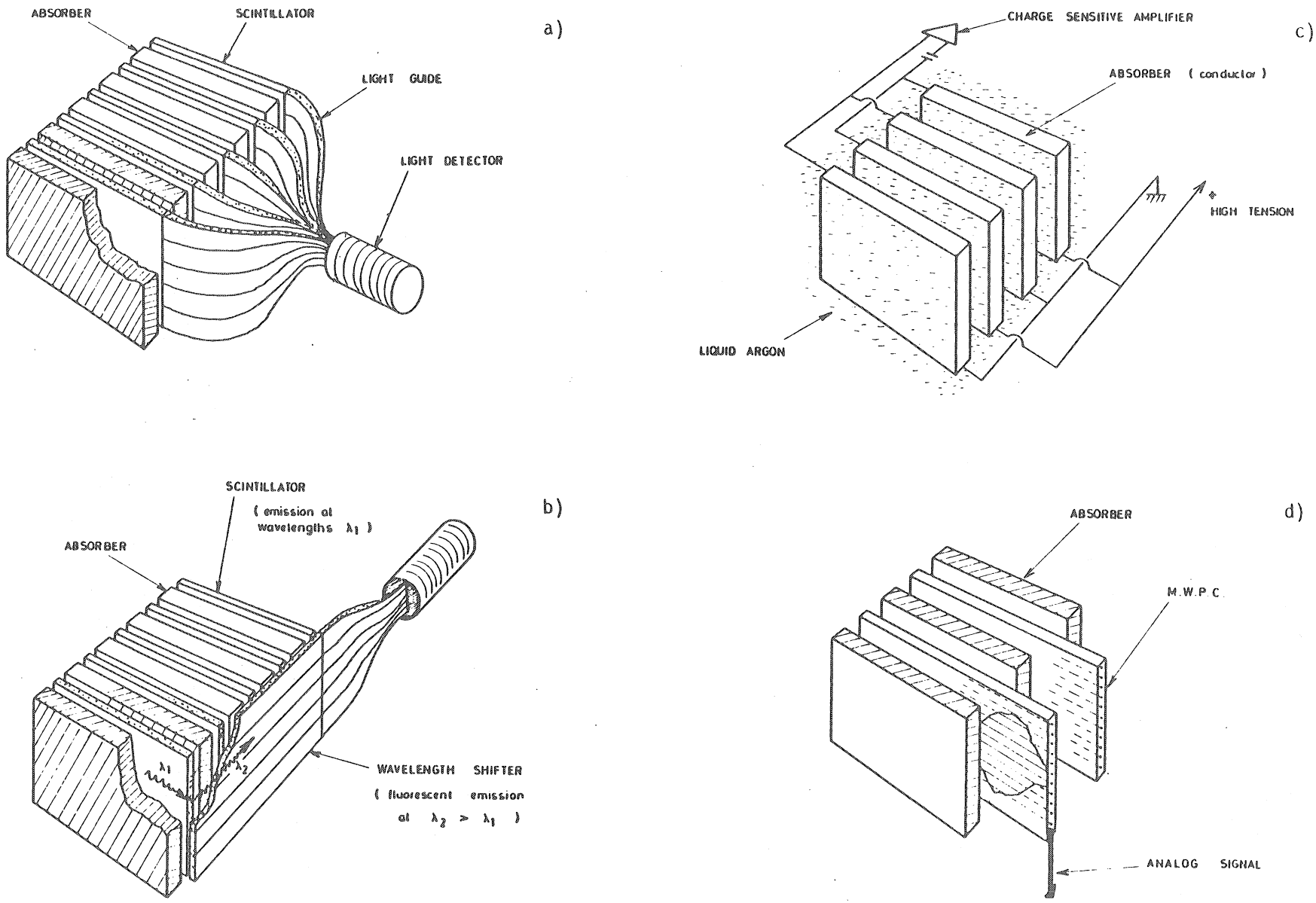
a)
ABSORBER
SCINTILLATOR
LIGHT GUIDE
LIGHT DETECTOR
b)
SCINTILLATOR
(emission at wavelengths λ_1)
ABSORBER
WAVELENGTH SHIFTER
(fluorescent emission at $\lambda_2 > \lambda_1$)
λ_1
λ_2
c)
CHARGE SENSITIVE AMPLIFIER
ABSORBER (conductor)
HIGH TENSION
LIQUID ARGON
d)
ABSORBER
M.W.P.C.
ANALOG SIGNAL

Fig. 12 (ref. [4])

is done through lucide light guides, where the emittance of the light emission has to be matched to the acceptance of the PM. The new method uses the process of wave length shifting (WLS), where scintillation light in the violet blue ($\lambda \simeq 400$ µm) is absorbed in a doped (trade name BBQ) plexi-sheet. Light is reemitted isotropically in the green ($\lambda \simeq 500$ µm) and travels to the PM. Only this compact technique (fig. 12(b)) permits the construction of densely packed calorimeter modules as needed today.

3.8 Hadron calorimeters

The principle involved in hadron calorimeters are inelastic hadronic collisions with the nuclei of the absorber, building up a nuclear cascade, with a mixed in π^0 component generating e.m. showers.

The mean free path in a hadronic shower is determined by the nuclear absorbtion length λ_{abs}, which depends only weakly on the material used

$$\lambda_{abs} = A/(N_A \sigma_{in}) \ [gcm^{-2}],$$

where $N_A = 6.10^{23}$ mole^{-1} and $\sigma_{in} \sim 30\ A^{0.75}$mb (pion) inelastic cross section.

Practical values are:

	Z	λ_{abs}	X_0	
H_2	1	56	63	[gcm^{-2}]
Fe	26	125	12	
Pb	82	190	6	

For dense material we find $\lambda_{abs} >> X_0$, and therefore hadron calorimeters have always to be sampling calorimeters, commonly consisting of iron-scintillator sandwiches, today with WLS read-out.

The resolution of hadron calorimeters depends on:

(i) Cascade containment (or leakage), which is important due to the long absorbtion length and the limited dimension of practical detectors.

(ii) Nuclear excitation, which absorbs part of the deposited energy, without corresponding emission of ionizing reaction products. Therefore, in the identical calorimeter electrons and hadrons of the same energy have different signal output S

$$S_{el}/S_{had} \sim 1.4.$$

(iii) Local fluctuations due to $\pi^0 \to \gamma\gamma$ initiated photon showers.

(iv) Sampling fluctuations.

Empirically the resolution of hadron calorimeters is

$$\sigma(E)/E \sim 0.5/\sqrt{E\,[\mathrm{GeV}]}.$$

3.9 Comparison of energy measurements

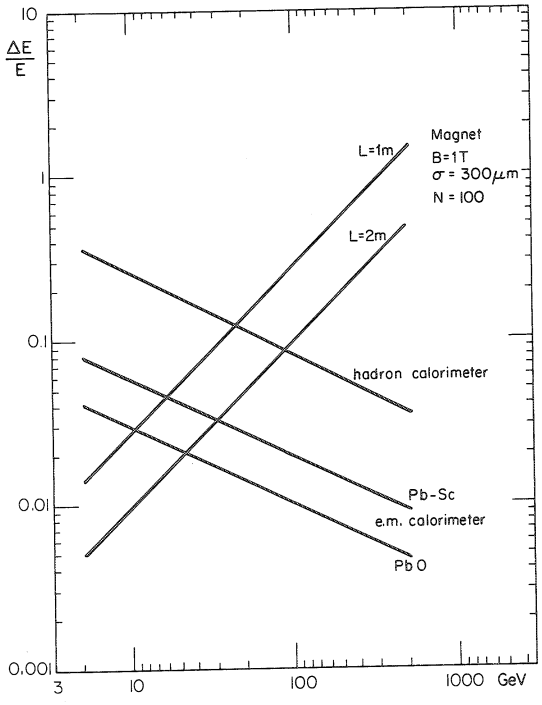

Fig. 13

Fig. 13 compares resolutions obtainable in the energy determination in electromagnetic and hadron calorimeters, and of momentum measurement in a magnet for two different useful lengths at a field of 1 Tesla.

3.10 Muon identification

The principle of muon identification relies on the property of penetration of matter, which is due to the absence of strong interaction and to the smallness of energy loss ghrough bremsstrahlung.

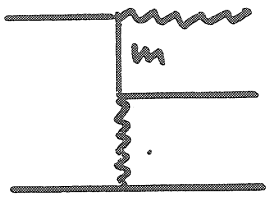

Intensity $\sim \frac{1}{m^2}$

$I_\mu/I_e = (m_e/m_\mu)^2 = 2.4\ 10^{-5}$

Muons, however, interact electromagnetically which leads to:

- energy loss through ionization of $dE/dx|_{min} \simeq 2.0$ MeV g^{-1} cm^2 in iron giving a limited range of 550 gcm^{-2} GeV^{-1}, leading to an energy cut-off in penetration;
- Coulomb scattering, i.e. limiting precision of angle determination after passage of the absorber.

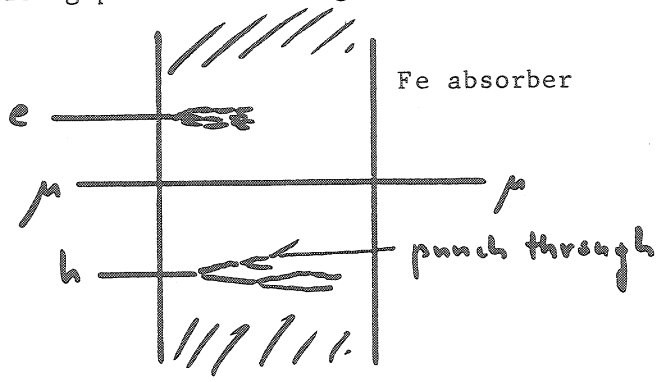

Most important background processes which result in penetrating particles simulating a muon are:

- <u>punch through</u> of a hadron, with a probability of $\exp(-x/\lambda_{abs})$, i.e. for 1 m $\hat{=}$ 720 gcm^{-2} of iron: $\exp(-5) \simeq 0.006$;

- <u>decay</u> of an unstable hadron (K,π) into a penetrating muon, with a probability $(1-\exp(-x/\lambda_{decay}))$ BR $\simeq xBR/\lambda_{decay}$, i.e. for a $K^{\pm} \rightarrow \mu\nu$, with BR = 0.635 and

$$\lambda_{decay} = \beta\gamma c\tau = \frac{p}{m} c\tau = p \cdot 7.4 \text{ [m]}$$

at 50 GeV, the probability is $\sim 2.10^{-3}$ to decay over one metre of flight path into a muon.

4. $p\bar{p}$ DETECTORS

In this section we describe the five specific detectors, as they were constructed for experiments UA1 to UA5 (UA is an abbreviation of Underground Area).

The experiments are located in two Long Straight Sections (LSS) on the SPS Ring (fig. 14)

LSS5: UA1 and UA3,

LSS4: UA2 or UA5, and UA4.

The summaries of these experiments are taken from the catalogue "Experiments at CERN in 1981" (also called Grey Book), edited by Y. Goldschmidt-Clermont.

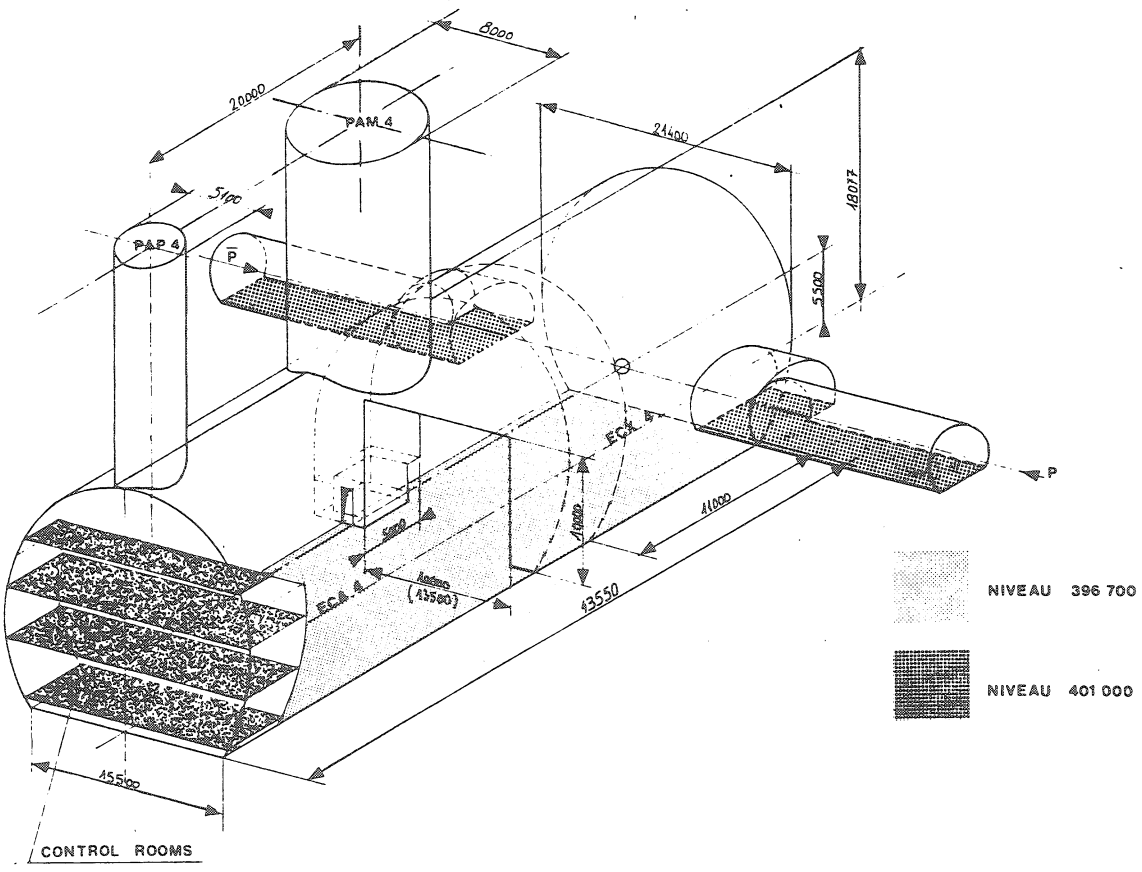

Design of the underground experimental area in LSS4

Fig. 14

4.1 UA1 - A 4π Solid Angle Detector for the SPS Used as a $p\bar{p}$ Collider at a Centre of Mass Energy of 450 GeV

Expt.	:	UA1
Beam	:	LSS5
Approved	:	29.06.1978
Status	:	Setting Up

A 4 π SOLID ANGLE DETECTOR FOR THE SPS USED AS A PROTON-ANTIPROTON COLLIDER AT A CENTRE-OF-MASS ENERGY OF 540 GeV

Aachen[1]-Annecy (LAPP)[2]-Birmingham[3]-CERN[4]-London (QMC)[5]-Paris (Coll. de France)[6]-Riverside[7]-Rome[8]-Rutherford Lab.[9]-Saclay (CEN)[10]-Vienna[11] Collaboration

G. Arnison[9], A. Astbury[9], B. Aubert[2], C. Bacci[8], R. Bernabei[8], A. Bézaguet[4], R. Böck[4], M. Calvetti[4], P. Catz[2], S. Centro[4], B. Chertok[4], F. Ceradini[8], J. Ciborowski[10], S. Cittolin[4], A.M. Cnops[4], C. Cochet[10], J. Colas[2], M. Corden[3], D. Dallman[11], S. D'Angelo[8], M. DeBeer[10], M. Della Negra[2], M. Demoulin[4], D. Denegri[10], D. DiBitonto[4], L. Dobrzynski[6], J. Dowell[3], M. Edwards[3], K. Eggert[1], E. Eisenhandler[5], N. Ellis[3], P. Erhard[1], H. Faissner[1], G. Fontaine[6], R. Frey[7], R. Fruhwirth[11], J. Garvey[3], S. Geer[4], P. Ghez[4], C. Ghesquiere[6], K.L. Giboni[1], R. Gibson[5], Y. Giraud-Heraud[6], A. Givernaud[10], A. Gonidec[2], G. Grayer[9], P. Gutierrez[7], R. Haidan[4], T. Hansl-Kozanecka[1], W.J. Haynes[9], R. Hertzberger[1], C. Hodges[7], D. Hoffmann[1], H. Hoffmann[4], D. Holthuizen[1], R.J. Homer[3], A. Honma[5], W. Jank[4], P. Kalmus[5], V. Karimaki[4], R. Keeler[5], I. Kenyon[3], A. Kernan[7], R. Kinnunen[4], H. Kowalski[4], W. Kozanecki[7], D. Kryn[6], F. Lacava[4], J.P. Laugier[10], J.P. Lees[2], H. Lehmann[1], R. Leuchs[1], A. Lévêque[10], D. Linglin[2], E. Locci[10], G. Maurin[4], T. McMahon[3], J.P. Mendiburu[6], M.N. Minard[2], G. Piano Mortari[4], M. Moricca[8], H. Muirhead[4], F. Muller[4], Y. Muraki[4], A.K. Nandi[9], L. Naumann[4], A. Norton[4], A. Orkin-Lecourtois[6], L. Paoluzi[8], M. Pernicka[11], G. Petrucci[4], M. Pimia[4], A. Placci[4], P. Queru[4], E. Radermacher[1], H. Reithler[1], J. Rich[10], M. Rijssenbeek[4], C. Roberts[9], C. Rubbia[4], J. Sass[10], B. Sadoulet[4], G. Sajot[6], G. Salvi[5], G. Salvini[8], J. Saudraix[10], A. Savoy-Navarro[10], D. Schinzel[4], W. Scott[9], T. Shah[9], M. Spiro[10], J. Strauss[11], K.S. Sumorok[3], C. Tao[4], G. Thompson[5], E. Tscheslog[1], J. Tuominiemi[4], H. Verweij[4], J.P. Vialle[4], J. Vrana[6], V. Vuillemin[4], H. Wahl[11], P. Watkins[3], J. Wilson[3], R. Wilson[4], M. Yvert[2], E. Zurfluh[4]

$p\bar{p}$ collisions in the SPS open up an energy domain, in which new and fundamental phenomena should emerge. At $\sqrt{s}$ = 540 GeV and L ≈ 10^{30} $cm^{-2}sec^{-1}$ the intermediate vector bosons and possible the Higgs boson(s) should be produced in detectable quantitities. Eventually new high-mass vector mesons and free quarks could be detected. At lower luminosities significant investigations can be carried out on quark-quark interactions through high p_T jets and Drell-Yan mechanism. Gluon interactions may be observed. In this new energy domain even "conventional" hadron physics takes on a renewed interest, especially in view of the possible change of régime suggested by cosmic-ray experiments.

The apparatus to study these phenomena will cover essentially all of the solid angle (down to 1°). The core of the apparatus is a conventional dipole magnet (7 kG) whose inner volume is occupied by a multiparticle detector, 6 m long and 1.3 m in radius, surrounded by a high-precision electromagnetic calorimeter. Hadron calorimetry is built inside the iron of the magnet, which also serves as a muon filter. In this way all the hadrons and charged leptons can be measured and electrons and muons distinguished from hadrons. The electron and hadron calorimeters provide selective triggers for W-search and jet studies.

References:

SPSC/78-6/P 92; 78-141/M 142; 78-158/M 146; 80-101/M 260

The reactions and the corresponding event configurations in the UA1 Detector are

- production and electronic decay of intermediate bosons

$\bar{p}p \to Z^0, W^\pm + \ldots$

$W^\pm \to e^\pm \nu$

$Z^0 \to e^+ e^-$

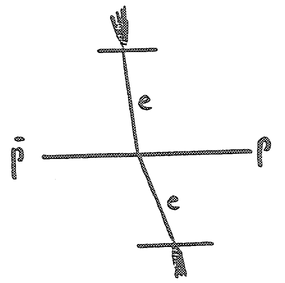

- production and muonic decay of intermediate bosons

$\bar{p}p \to Z^0, W^\pm + \ldots$

$W^\pm \to \mu^\pm \nu$

$Z^0 \to \mu\mu$

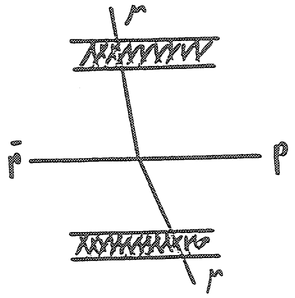

- quark-quark scattering

$\bar{p}p \to \bar{q}q$ + hadrons

$\quad \to$ jets of hadrons

and other hadronic processes.

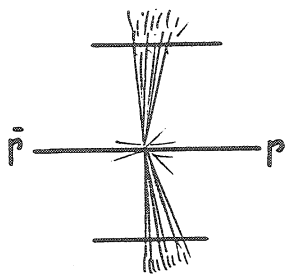

They require a complete detector with magnetic field, central track detector, photon and hadron calorimeters, electron and muon identification, over a large acceptance with appropriate (mass) resolution.

The elements, and their parameters, of the UA1 experiment (figs 15-16) are:

4.1.1 The magnet - a dipole with horizontal field, with a useful volume of LxWxH = 7.0 x 3.5 x 3.5 m^3 with a field of 0.7 Tesla at 6 MW and a weight of 1460 t. The dipole field acts on the circulating beams and is compensated for by up and downstream compensators of 2 x 2.5 Teslametre at ±8 m distance (fig. 17).

4.1.2 The central detector (CD) - is an image chamber consisting of 6 half-cylinders with dimensions of LxR = 1.93 x 1.1 m^2, thus forming a cylinder of $\sim$ 6 m length and 2.2 m diameter. The orientation of the wire planes is such that drift and sagitta coincide (fig. 18-19). The drift gap is 18 cm wide, the sense wire pitch is 6 mm, the HV is -28 kV, i.e. 1.6 kV/cm, with a gas filling of 40% argon and 60% ethane. The 6000 sense wires are read out with charge division and dE/dx measurement by means of a Charge and Time Digitizer (CTD). The expected resolutions are 200 µm in drift and 1% in charge division. The drift angle is 23° with respect to the electric field at 0.7 Tesla.

4.1.3 The electromagnetic calorimeter - is of lead-scintillator sandwich type, 25 radiation length thick, 120 layers of 1.2 mm lead and 1.5 mm scintillator, with 4 samplings, WLS read-out into 1024 PM channels. Geometrically:

- the central region > 30° (< 150°) is covered by 48 "gondolas" (fig. 20);
- the forward cones > 5° (< 175°) are covered by 2 "bouchons", each with 32 wedges of sandwich counters and $\sim$ 2000 crossed proportional tubes of 1 cm Ø for position measurement.

The resolutions are

$\sigma(E)/E = 0.15/\sqrt{E}$ (measured)

$\sigma_Z \simeq 2$ cm, from attenuation in the scintillator when read from both sides

$\sigma_{r\emptyset} \simeq 20$ cm, from attenuation in WLS, when read out from both sides.

4.1.4 The hadron calorimeter (fig. 21) - consists of the sliced iron yoke of the magnet "calorimetrized magnet", with slices of 49 mm of iron, followed by 10 mm of scintillator, in total 80 cm of iron, which corresponds to $\sim$ 5 absorbtion lengths. Two samplings are read by means of WLS into 1250 PM channels. Geometrically the magnet is composed of 16 azimuthal C modules and 12 endcap I modules, covering a total detection volume of LxHxW = 11.0 x 6.4 x 6.0 m^3, with detection cells of 1.0 x 0.9 x 0.9 m^3. The acceptance is total above 5°, the resolutions are $\sigma(E)/E = 0.8/\sqrt{E}$ in energy, whereas the spatial resolution is that of a cell size.

4.1.5 The muon detector - consists of 50 chambers with 6000 drift tubes, each chamber with dimensions 5.8 x 4.8 m^2, with (2+2) orthogonal layers of drift tubes (15 x 5 cm^2), arranged in two chamber layers with 60 cm distance in between, covering a total surface of 450 m^2. The tubes are operated with the CD gas (40% argon, 60% ethane) at -7.5 kV, i.e. 1 kV/cm, and they are read-out with a Multi-Time Digitizer (MTD) circuit.

4.1.6 The forward spectrometers - consist of one forward and one very forward detector on each side. They are composed of

- an image drift chamber for track measurement,
- an electromagnetic calorimeter, and
- a hadron calorimeter (CALCOM = calorimetrized compensator), the latter with dimensions of LxWxH = 3.5 x 2.0 x 2.0 m^3.

Fig. 22 shows one of the first $\bar{p}p$ events in the central detectors.

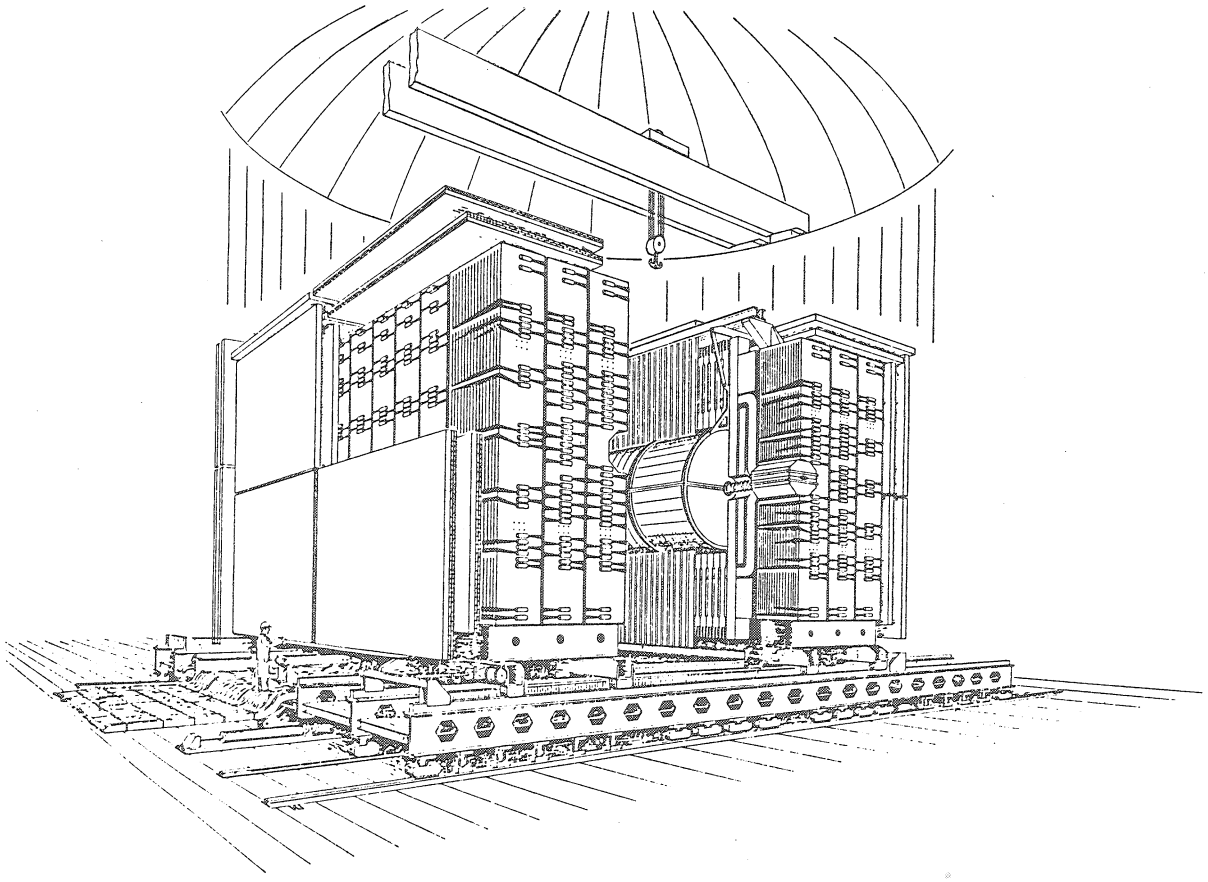

Fig. 15

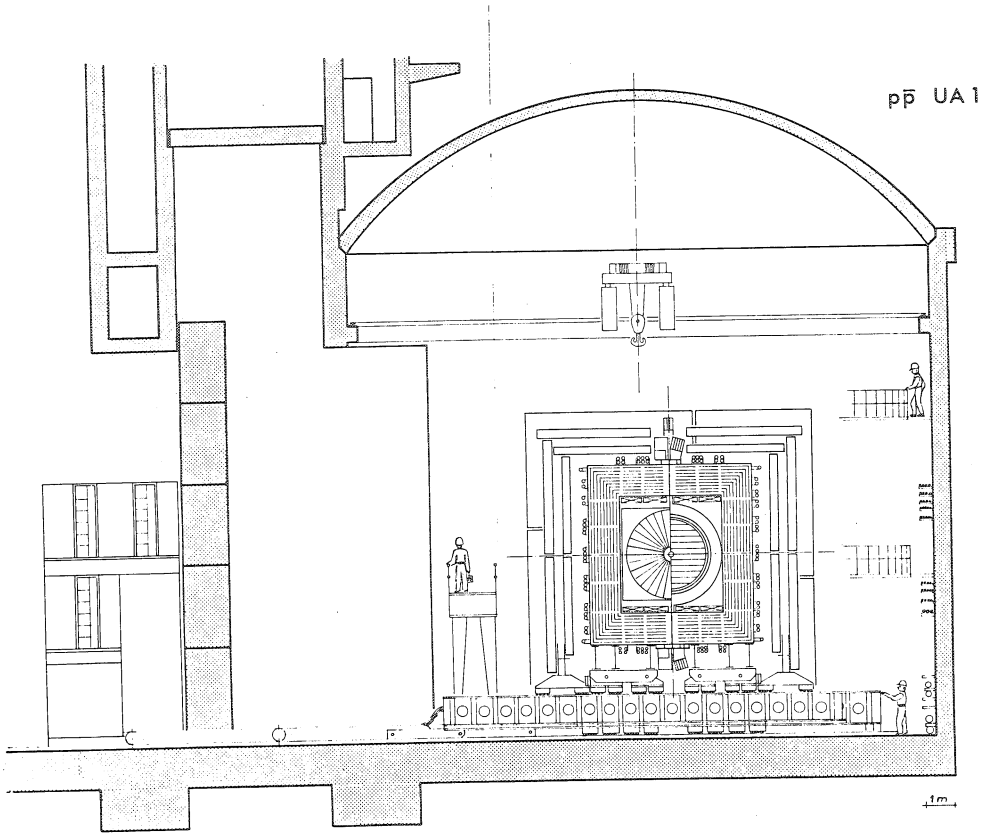

Fig. 16

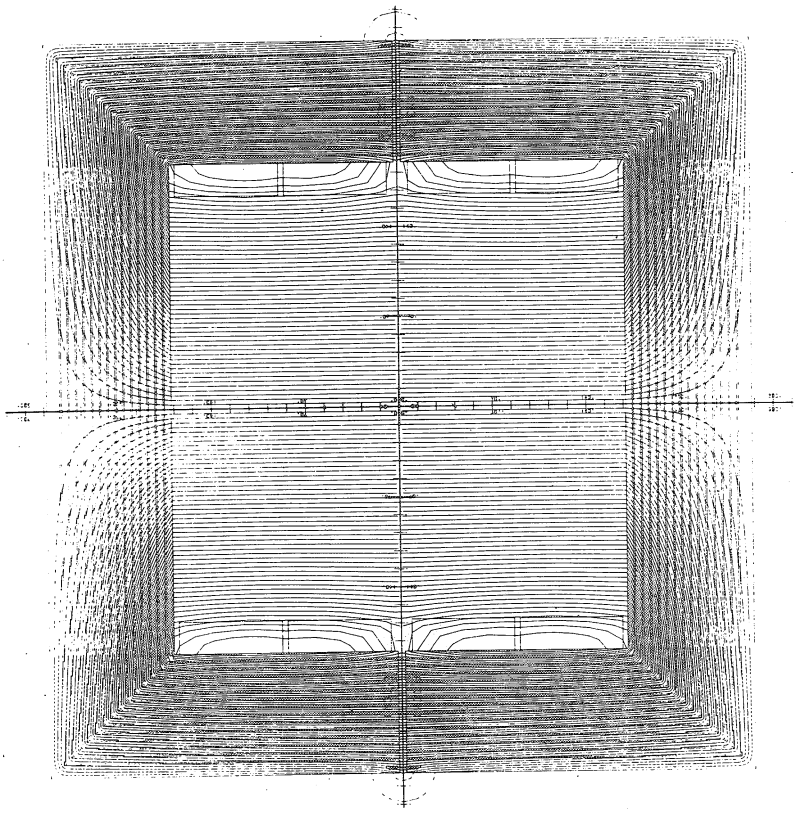

Fig. 17

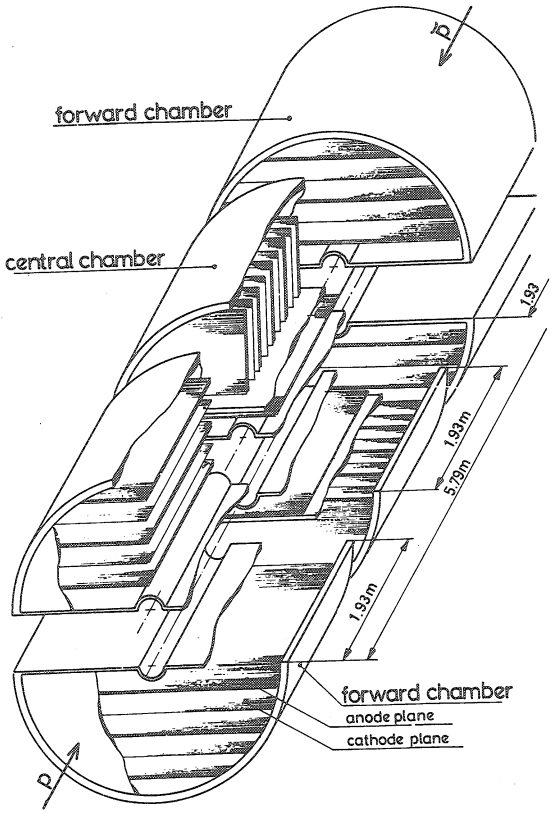

Fig. 18

FORWARD CHAMBER

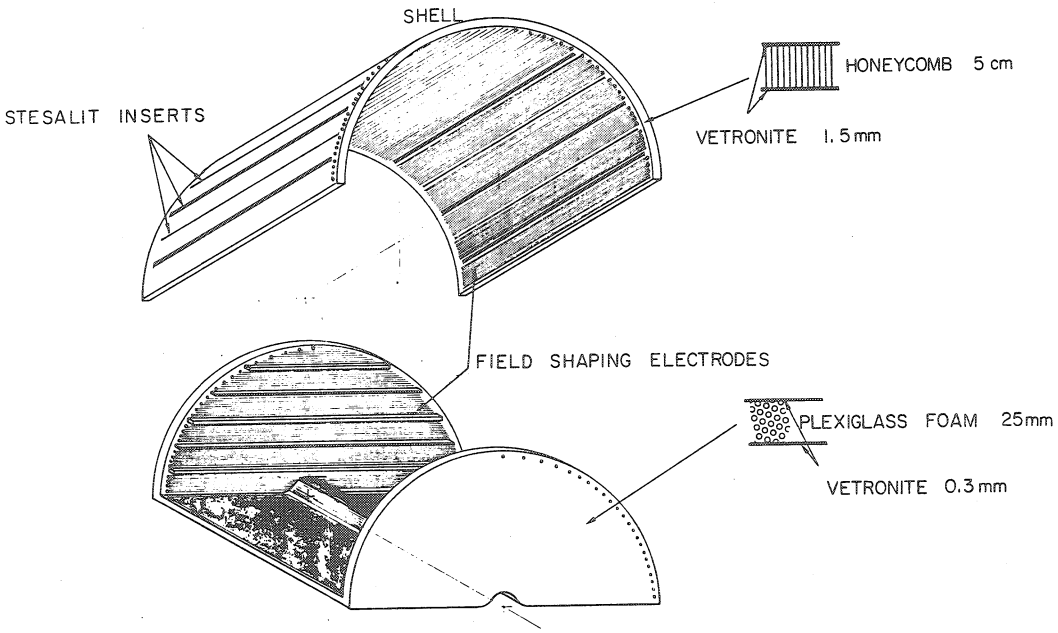

Fig. 19

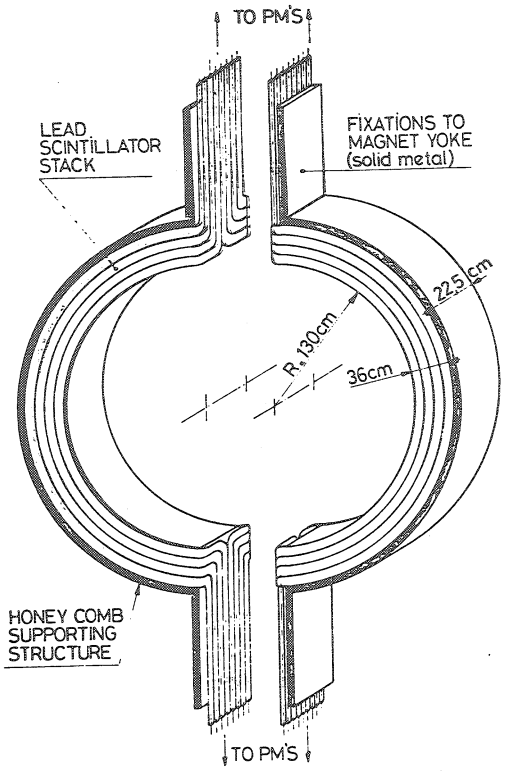

Schematic of the large angle unit photon detector.

Fig. 20

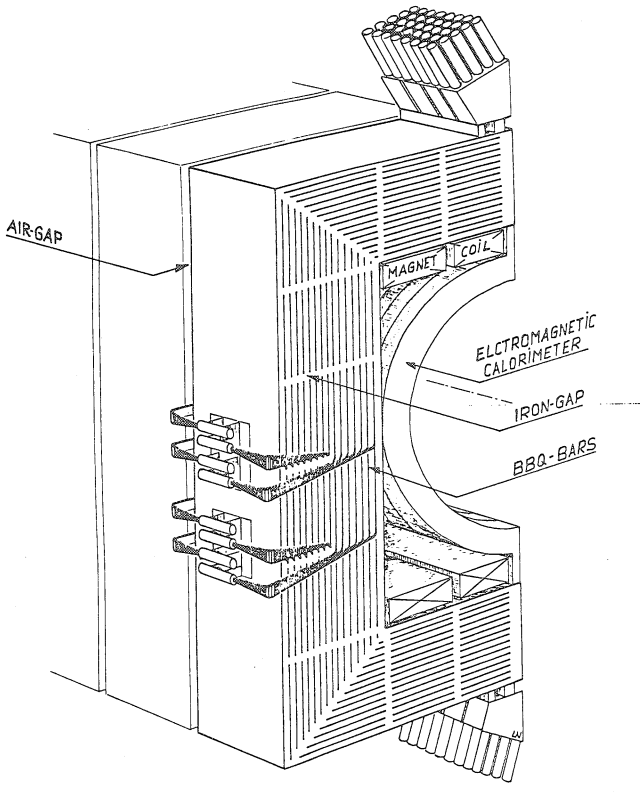

Fig. 21

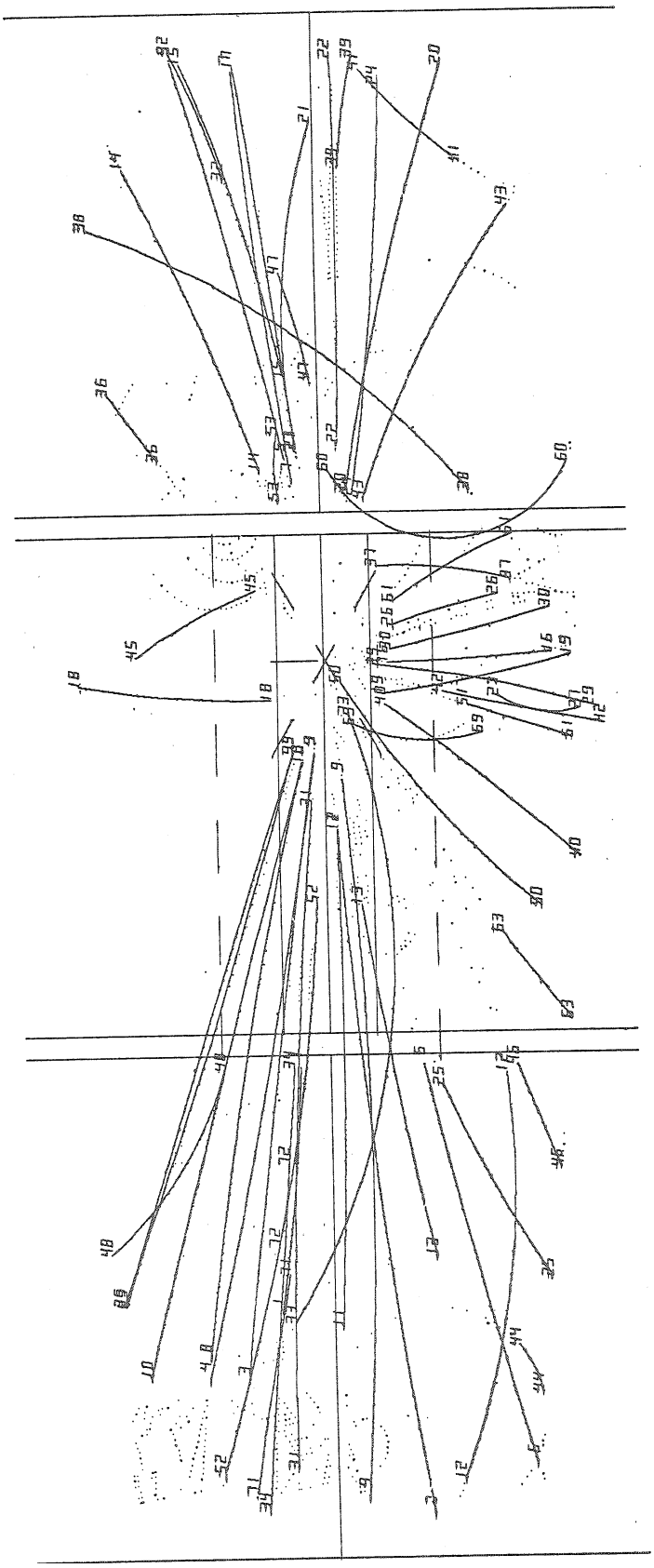

Fig. 22

4.2 UA2 - Study of $\bar{p}p$ Interactions at 540 GeV c.m. Energy etc.

Expt.	: UA2
Beam	: LSS4
Approved	: 14.12.1978
Status	: Setting Up

STUDY OF ANTIPROTON-PROTON INTERACTIONS
AT 540 GeV c.m. ENERGY

Bern[1]-CERN[2]-Copenhagen[3]-Orsay (LAL)[4]-Pavia[5]-Saclay (CEN)[6] Collaboration

M. Banner[6], P. Bloch[6], F. Bonaudi[2], K. Borer[1], M. Borghini[2], C. Bruneton[6], J.C. Chollet[4], A.G. Clark[2], C. Conta[5], P. Darriulat[2], L. Di Lella[2], P.A. Dorsaz[2], L. Fayard[4], M. Fraternali[5], D. Froidevaux[4], J.M. Gaillard[4], O. Gildemeister[2], G. Goggi[5], B. Hahn[1], H. Hänni[1], J.D. Hansen[2], J.R. Hansen[2], P. Hansen[3], T. Himmel[2], V. Hungerbühler[2], P. Jenni[2], O. Kofoed-Hansen[3], M. Livan[5], C. Loucatos[6], B. Madsen[3], B. Mansoulie[6], G.C. Mantovani[5], L. Mapelli[5], B. Merkel[4], R. Møllerud[3], G. Parrour[2], F. Pastore[5], H. Plothow[4], J.P. Repellin[4], A. Rimoldi[5], A. Rothenberg[2], G. Sauvage[4], J. Schacher[1], J. Teiger[6], H. Zaccone[6], W. Zeller[1]

The purpose of this experiment is to detect the production and decay of $W^{\pm}$ and Z^0 bosons at the SPS $\bar{p}p$ facility. The design of the apparatus combines large solid angle coverage, with compactness and simplicity of operation. It includes electromagnetic and hadronic calorimetry in the central region and magnetic spectrometers in the forward and backward cones equipped for electron detection. In addition a small azimuthal wedge in the central region is instrumented to cover other aspects of $p\bar{p}$ collisions when the collider luminosity has not yet reached its design value.

References:
SPSC/78-8/P 93; 78-54/P 93/Add.1; 78-126/M 139; 78-133/M 141; 78-162/M 147; 79-27/M 155; 80-96/M 255; 80-104/M 255/Add. 1

Reactions and event configurations in the UA2 detector are the following:

- production and electronic decay of intermediate bosons

$$\bar{p}p \rightarrow Z^0,\ W^{\pm} + \ldots,$$
$$\qquad\quad \hookrightarrow e^{\pm}\nu$$
$$\qquad\quad \hookrightarrow e^{+}e^{-}$$

- electron charge assymetry in the decay of the forward $W^{\pm}$ boson,

- quark-quark scattering and other hadronic processes

$$pp \rightarrow qq + \text{hadrons}$$
$$\qquad\quad \hookrightarrow \text{hadrons, hadron jets.}$$

This needs a detector with calorimeters for electrons and hadrons with high acceptance and resolution, and magnetic field in the forward directions for charge determination.

The elements, and their parameters, of the UA2 detector are (fig. 23-24):

4.2.1 The vertex detector - a (mixed type) cylindrical wire chamber, consisting of 5 layers of MWPC with supplementary inclined cathode strip read-out, and JADE type drift chamber, the latter with two layers with 2 x 24 cells ($\Delta\phi$ = 15°) and a total of 288 wires. The external dimensions of the cylinder are LxR = 2.0 x 0.37 m^2, the acceptance is complete in diameter, for $\theta > 20°$ ($\theta < 160°$).

4.2.2 The central calorimeter (fig. 25) - is a combined electromagnetic and hadron calorimeter, composed of 24 "orange slices" of 10 cells each, i.e. 240 cells of $\Delta\theta$ = 10°, $\Delta\phi$ = 15°. A calorimeter cell contains:

- an electromagnetic sector of 26 x (3.5 mm Pb + 4 mm Sc), 18 Xo,
- a hadron sector of 40 x (15 mm Fe + 5 mm Sc), 4.5 λ_{abs}, and
- 3 samplings with WLS read-out.

The acceptance is complete in diameter for $\theta > 40°$ ($< 140°$). The resolution is

- electro-magnetic $\sigma(E)/E = 0.15/\sqrt{E}$,
- hadron $\sigma(E)/E = 0.75/\sqrt{E}$.

4.2.3 The forward/backward detector - covering the full area for $20° \lesssim \theta \lesssim 37.5°$ ($142.5° \lesssim \theta \lesssim 160°$) and consisting of three components:

- Toroidal magnets, composed of 12 coils each, generating a magnetic field of 0.31 Teslametre, with a deflection of 0.1/p[GeV/c] and serving for charge determination only.
- Drift chambers for charged particle track measurement, on each side 12 telescopes with 3 drift chambers of 3 planes in a telescope. The vertex detector is used as initial stage of a telescope.
- Electro-magnetic calorimeters of the lead-scintillator type, segmented on each side into 120 (24 x 5) independent detector cells with $\Delta\theta = 3.5°$, $\Delta\phi = 15°$. The calorimeter modules are preceded by a lead converter with crossed proportional tubes for position measurement.

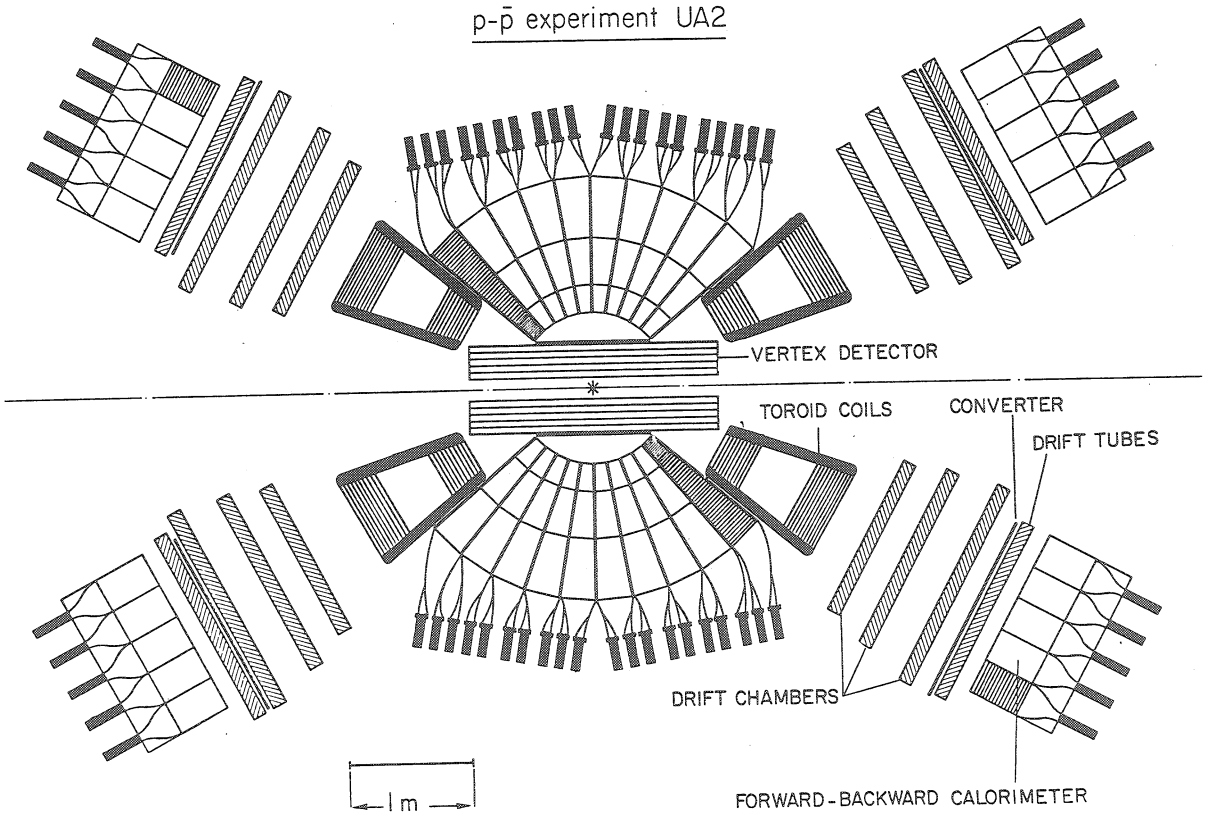

Fig. 23

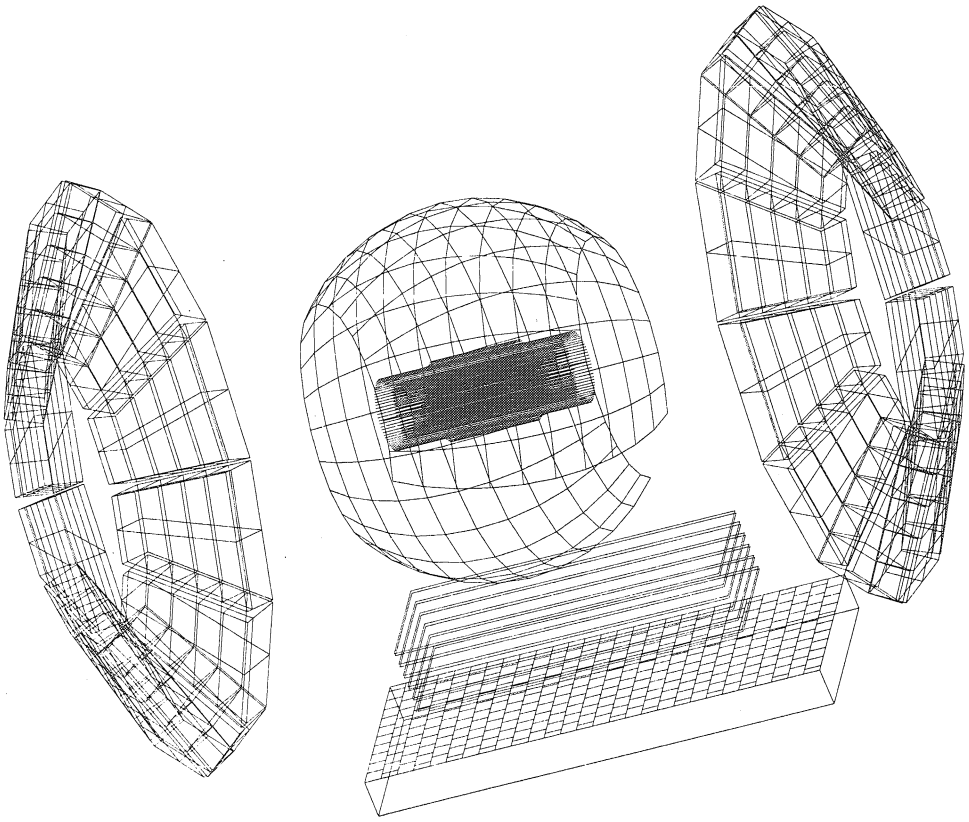

Fig. 24

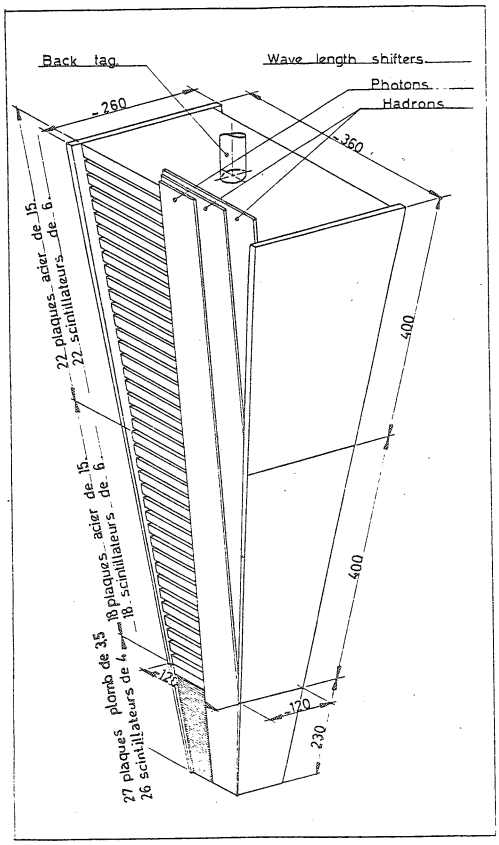
Back tag
Wave length shifters
Photons
Hadrons
260
360
400
400
120
230
22 plaques acier de 15
22 scintillateurs de 6
18 plaques acier de 15
18 scintillateurs de 6
27 plaques plomb de 3,5
26 scintillateurs de 4

Fig. 25

4.3 UA3 - Search for Magnetic Monopoles at the $\bar{p}p$ Colliding Ring etc.

Expt.	: UA3
Beam	: LSS5
Approved	: 14.12.1978
Status	: Preparation

SEARCH FOR MAGNETIC MONOPOLES
AT THE $\bar{p}p$ COLLIDING RING

Annecy (LAPP)[1]-CERN[2]

B. Aubert[1], P. Musset[2], M. Price[2], J.P. Vialle[2]

The aim of this experiment is to investigate the existence of particles carrying isolated magnetic charges at the $\bar{p}p$ colliding ring. Such particles can be detected by solid state track detectors placed in a magnetic field and developed by subsequent chemical etching. In order to avoid possible interactions with matter, the detection is simultaneous with the production and presence of substance is suppressed to the greatest possible extent between the production region and the detectors. A good sensitivity over a large range of magnetic charge values, the natural unit of which is the Dirac change

$$g_D = \tfrac{1}{2} \frac{\hbar c}{e} ,$$

is an important feature of the design. The high energy available at the $\bar{p}p$ colliding ring allows to reach high mass values.

Detailed study of the quality of the vacuum permitted to install detectors directly inside the vacuum pipe. Other detectors are being installed inside the UA1 apparatus.

References:
SPSC/78-15/P 96 ; 78-74/M 116

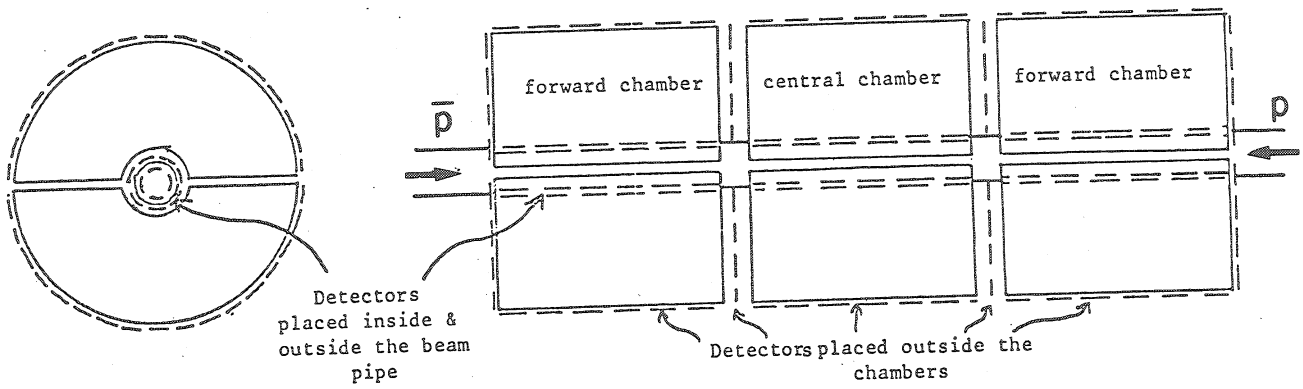

PLASTIC LAYER DETECTOR 50 μm KAPTON FOILS

Fig. 26

4.4 UA4 - Measurement of Elastic Scattering and of Total Cross Section at the CERN $\bar{p}p$ Collider etc.

Expt.	: UA4
Beam	: LSS4
Approved	: 18.1.1979
Status	: Setting Up

MEASUREMENT OF ELASTIC SCATTERING AND OF TOTAL CROSS-SECTION AT THE CERN $\bar{p}p$ COLLIDER

Amsterdam[1]-CERN[2]-Genova[3]-Napoli[4]-Pisa[5] Collaboration

R. Battiston[5], M. Bozzo[3], P.L. Braccini[5], F. Carbonara[4], R. Carrara[5], R. Castaldi[5], F. Cervelli[5], G. Chiefari[4], A.N. Diddens[1], E. Drago[4], M. Haguenauer[2], B. Koene[1], L. Linssen[1], G. Matthiae[4], L. Merola[4], M. Napolitano[4], V. Palladino[2], F. Silombra[3], G. Sanguinetti[5], C. Sciacca[4], G. Sette[3], J. Timmermans[1], R. Urbani[3], C. Vannini[2], R. Van Swol[1], J. Velasco[2], F. Visco[4]

The aim of the experiment is to measure elastic scattering and the total cross-section at the $\bar{p}p$ collider.

The experimental apparatus is composed of two parts:

1) Telescopes of high accuracy drift chambers, inserted into moveable sections of the vacuum chamber ('Roman pots'), will detect elastic scattering in the angular region from a few tenths of mrad up to about 3 mrad.

2) A large system of drift chambers and counter hodoscopes covering $\sim 4\pi$ ('vertex detector') will measure the total inelastic rate.

By combining the two measurements, the total cross-section will be obtained with accuracy at the 1% level.

References:
SPSC/78-105/P 114; 78-11/I 100; 79-10/P 114/Add.1; 80-14/P 114/Add.2; 80-59/M 236

Note: The experiment UA4 intends to measure

$$\text{elastic cross sections } \frac{d\sigma}{dt}\Big|_{el} = \frac{dN_{el}}{dt} \cdot \frac{1}{L}$$

$$\text{total cross sections } \sigma_{tot} = N_{tot} \cdot \frac{1}{L}$$

Both independent measurements require the knowledge of the luminosity L. The optical theorem

$$\sigma_{tot} = \sqrt{16\pi \lambda\!\!\!^{-2} \frac{ds}{dt}\Big|_{t=0}}$$

permits to determine σ_{tot} by measurement of N_{tot} and $\frac{dN}{dt}$ $(t = -4E^2 \sin^2 \frac{\theta}{2})$ without knowledge of L

$$\sigma_{tot} = 16\pi \lambda\!\!\!^{-2} \frac{dN}{dt}\Big|_{t=0} / N_{tot} \cdot$$

UA4

THE 4π DETECTOR

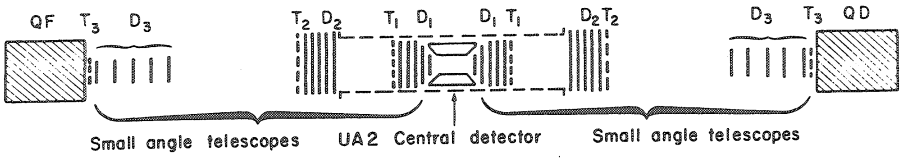

ELASTIC SCATTERING SETUP

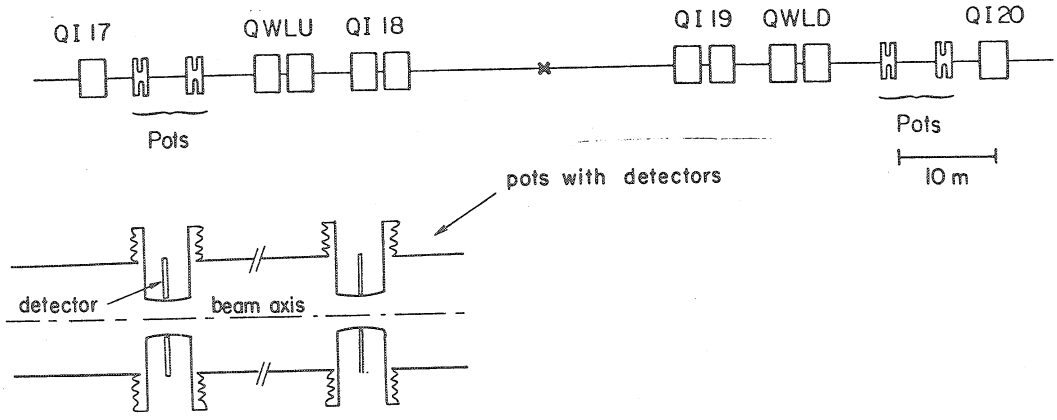

Experiment UA4 : Measurement of Elastic Scattering and Total Cross-Section at the CERN $\bar{p}p$ Collider

Fig. 27

4.5 UA5 - Investigation of $p\bar{p}$ Events at 540 GeV c.m. Energy with a Streamer Chamber Detection System

Expt.	: UA 5
Beam	: LSS4
Approved	: 15.2.1979
Status	: Setting Up

INVESTIGATION OF PROTON-ANTIPROTON EVENTS AT 540 GeV c.m. ENERGY WITH A STREAMER CHAMBER DETECTION SYSTEM

Bonn[1]-Brussels[2]-Cambridge[3]-CERN[4]-Stockholm[5] Collaboration

K. Alpgard[5], R.E. Ansorge[3], B. Asman[5], S. Berglund[5], D. Bertrand[2], K. Böckmann[1], C.N. Booth[3], L. Burow[1], P. Carlson[5], J.R. Carter[3], B. Eckart[1], G. Ekspong[5], K. French[3], J. Gaudaen[2], M. Gijsen[2], K. v. Holt[1], R. Hospes[1], D. Johnson[2], K. Jon-And[5], T. Kokott[1], M.N. Maggs[3], R. Meinke[1], H. Mulkens[2], Th. Müller[1], D.J. Munday[3], A. Odian[4](*), M. Rosenberg[1], J.G. Rushbrooke[3], H. Saarikko[1], T. Saarikko[1], F.A. Triantis[4](**), C. Walck[5], C.P. Ward[3], D.R. Ward[3], G. Weber[4](***), A.R. Weidberg[3], T.O. White[3], G. Wilquet[2], N. Yamdagni[5]

The SPS collider offers an opportunity to study hadronically-produced events in a new energy domain where cosmic ray experiments have suggested the existence of entirely new phenomena. Of particular interest are the so-called "Centauro" events, thought to be characterized by very large charged multiplicities ($\langle n_c \rangle \sim 10^2$) and by very few accompanying neutral particles.

Two large (6 m long) streamer chambers, triggered by hodoscopes of scintillation counters at either end and at 90^0, and viewed by cameras via image intensifiers, are to be installed in the collider intersection region LSS4. Charged tracks will be observed down to $3/4^0$, and hence over most of the pseudo-rapidity range ($|\eta| < 5.0$) to be expected for high multiplicity events. Lead-glass plates will be placed within the chambers to convert γ's produced within the same η-range. This apparatus is to afford a rapid visual survey of this new energy region, and permit a search for Centauro-type events with high efficiency.

(*) Visitor from SLAC
(**) Visitor from Ioannina, Greece
(***) Visitor from Hamburg University.

References:

SPSC/78-70/P 108; 78-107/P 108/Add.1; 78-147/P 108/Add.2; 79-11/M 153; 80-78/M 243

The UA5 detector is based on two streamer chambers, with dimensions of LxWxH = 6.0 x 1.25 x 0.5 m^3 (fig. 28).

The chambers are positioned above and underneath the vacuum chamber with colliding beams at a distance of ±4 cm from the beam axis.

The chambers are operated with a gas consisting of 90% neon, 9.5% helium, 0.5% isobutane and 10^{-7} SF6 with a HV pulse of 12 ns duration and 350 kV amplitude, i.e. 17 kV/cm (FWHM) electric field. The HV pulse is generated by a Marx generator and shaped by means of a Blumlein transmission line.

The chambers are viewed at with 2 x 3 cameras with 2000 fold image intensifiers of 90 mm diameter producing via mirrors 12 steroscopic photos with a demagnification of 50-80. The (measured) spatial resolution is < 2 mm, and the two track resolutions are of the same order. The streamer chamber HV is triggered on beam-beam interactions with two 6-plane scintillation hodoscopes (fig. 28).

Fig. 29 shows one of the first picture of a $\bar{p}p$ collision.

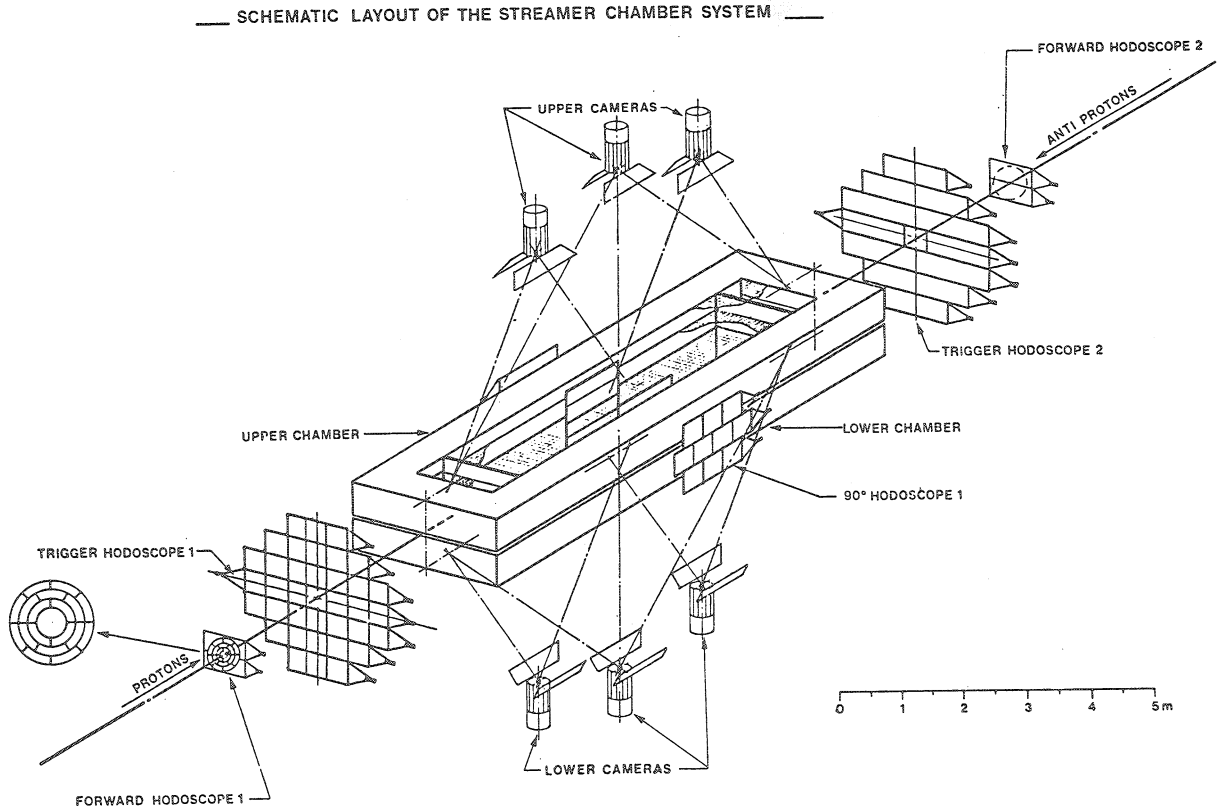

Fig. 28

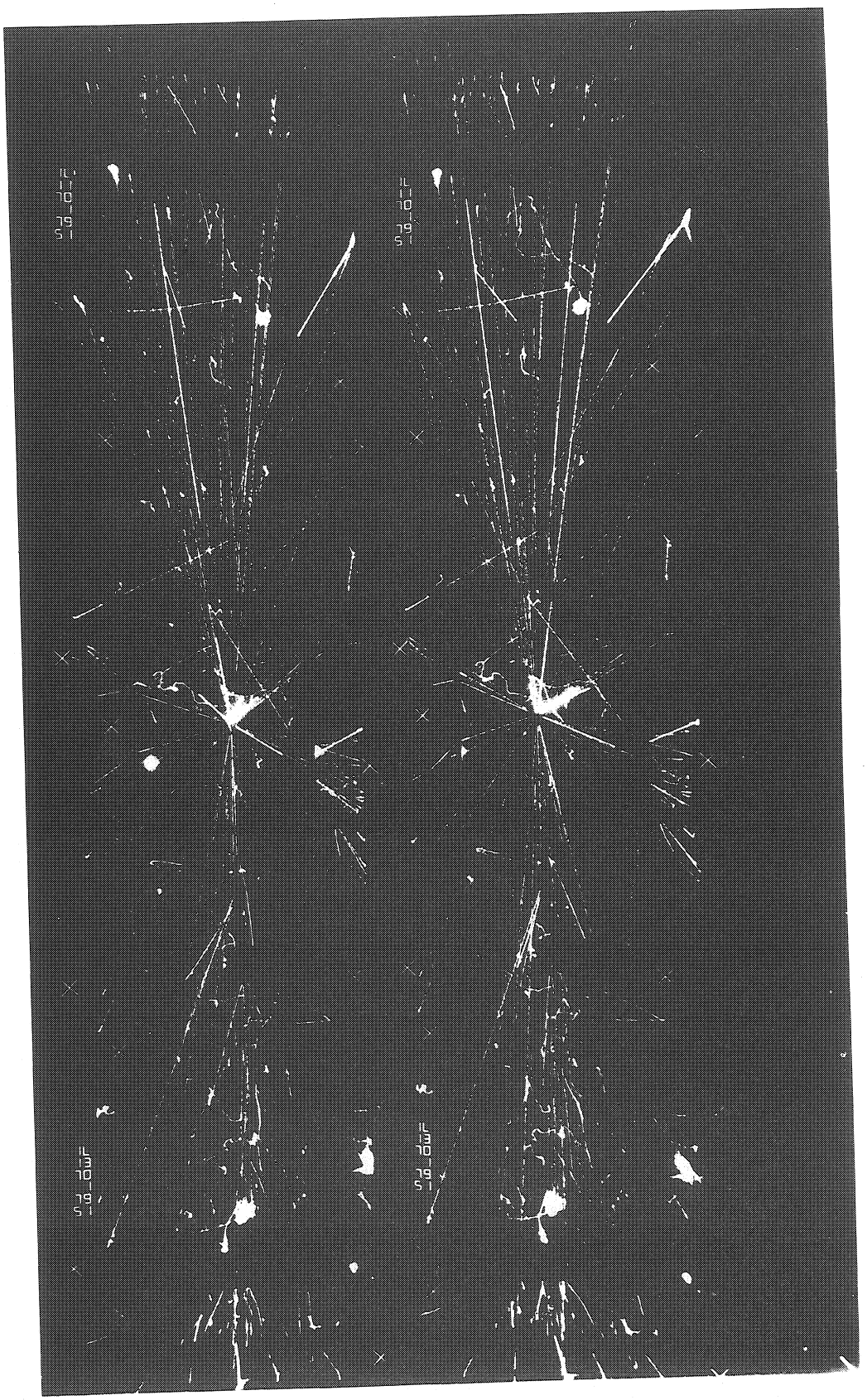

Fig. 29

Acknowledgements

The lecturer gratefully acknowledges the help of H.F. Hoffmann, L. Di Lella, P. Musset, G. Matthiae and R. Meinke concerning information on the experiments UA1 to UA5, respectively.

He also thanks H. Braun (Strasbourg), L. Jauneau (Orsay) and M. Nikolic (Beograd) for the hospitality at Kupari.

REFERENCES

No attempt is made to establish a complete list of references. We restrict ourselves to the complementary lectures at this school, and to the proposals for the $\bar{p}p$ experiments.

[1] Rol Johnson, CERN/PS/AA/Note 81-2.

[2] R. Horgan and M. Jacob, Kupari Lecture Notes 1981 (unpublished).

[3] G. Goggi, CERN/EP 81-8.

[4] Ch. Fabjan and H.G. Fischer, Rep. Progr. Phys. 43 (1980) 1003.

[5] A. Wagner, Physica Scripta, Proceedings from the International Conference on Experimentation at LEP, Uppsala (1980) p. 446.

[6] B. Sadoulet, Physica Scripta, Proceedings from the International Conference on Experimentation at LEP, Uppsala (1980) p. 434.